Solar Energy 310 (2026) 114474

Contents lists available at ScienceDirect

Solar Energy

journal homepage: www.elsevier.com/locate/solener

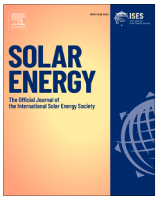

Valorizing reverse osmosis brine with solar energy: Modeling, simulation, and techno-economic comparison of PV/T- and PV-driven hybrid desalination systems incorporating membrane distillation

Paolo Vitulli [a,c,*], Alejandro Bueso Sánchez [b], Giulia Tanoni [a], Emanuele Principi [a], Stefano Squartini [a], Guillermo Zaragoza [b]

[a] Università Politecnica delle Marche, Department of Information Engineering, Via Brecce Bianche, 12, Ancona, 60131, Marche, Italy
[b] CIEMAT, Plataforma Solar de Almería, Ctra. de Senés, km. 4, 5, Tabernas, Almería, 04200, Spain
[c] Università di Salerno, Department of Information and Electrical Engineering and Applied Mathematics, Via Giovanni Paolo II, Fisciano, 84084, Italy

HIGHLIGHTS

- Placing MD plants in series with a RO unit enhances overall freshwater production and increases the RR.
- The solar-powered RO-MD system with energy storage achieves a lower LCOW than other solar-powered desalination options.
- A hybrid PV/T collector in an RO-MD system enables higher freshwater output than a standard PV collector.
- A hybrid PV/T collector in an RO-MD system yields a lower LCOW than a conventional photovoltaic collector.

ARTICLE INFO

Keywords:
Solar energy
Hybrid photovoltaic/thermal collector (PV/T)
Reverse osmosis desalination
Membrane distillation desalination
Energy storage

ABSTRACT

Seawater desalination provides an effective means to address water scarcity intensified by global warming and rising demand. When powered by solar energy, it can supply freshwater with minimal CO_2 emissions.

This study develops and compares two fully solar-powered desalination systems, using modeling and simulations, aimed at increasing the Recovery Ratio (RR) and valorizing brine from a Reverse Osmosis (RO) unit. Both systems integrate thermal and electrical energy storage and incorporate Membrane Distillation (MD) units operating in series with RO. System A uses photovoltaic (PV) panels and solar thermal (ST) collectors, while System B combines hybrid photovoltaic/thermal (PV/T) panels with ST collectors. Simulations are performed under real meteorological conditions over one year in Almería, Spain.

No previous work has assessed the techno-economic performance of solar-powered hybrid desalination systems with energy storage for higher RRs, nor compared traditional and hybrid solar collectors through dynamic annual simulations.

The RO–MD configuration enhances RR and freshwater production relative to RO alone. System A increases output by 9.22%, and System B by 8.60%. RR rises from 40.50% to 44.23% in System A and from 42.04% to 45.66% in System B.

PV/T integration in System B further improves performance by preheating seawater, reducing specific energy consumption (SEC), and increasing PV efficiency. This results in an 8.93% production gain and a 3.24% RR increase over System A.

Levelized Cost of Water (LCOW) values are 5.01 and 5.27 USD/m^3 for Systems B and A, respectively, higher than conventional water costs but lower than many reported for solar-powered desalination systems.

* Corresponding author at: Università Politecnica delle Marche, Department of Information Engineering, Via Brecce Bianche, 12, Ancona, 60131, Marche, Italy.
Email address: p.vitulli@pm.univpm.it (P. Vitulli).

https://doi.org/10.1016/j.solener.2026.114474
Received 14 October 2025; Received in revised form 20 February 2026; Accepted 23 February 2026
Available online 2 March 2026

Nomenclature

Latin symbols

$\bar{T}$	Mean Temperature [K]
$\dot{m}$	Mass flow rate [kg/s]
A	Area [m^2]
a	Amortization Factor [−]
C	Cost [USD]
c	Specific heat [J/(kgK)]
cde	Saving coefficient for consumption [kg/kWh]
E	Energy [kWh]
$F_{m,n}$	View Factor between layer m and n [−]
H	Thermal loss coefficient [J/(sK)]
$hc_{i,j}$	Conductive heat transfer coefficient between layers i and j [W/(m^2K)]
$hr_{i,j}$	Radiative heat transfer coefficient between layers i and j [W/(m^2K)]
$hv_{i,j}$	Convective heat transfer coefficient between layers i and j [W/(m^2K)]
I	Solar radiation [W/m^2]
J	Permeate flux of MD [L/(hm^2)]
k	Annual interest rate [−]
L	Flat plate tube length [m]
M	Mass [kg]
N	System lifetime [years]
n	Number of
n_a	Number of tubes in each solar thermal collector [−]
n_l	Number of solar thermal loop [−]
n_p	Number of solar thermal panels connected in parallel [−]
n_s	Number of solar thermal collectors connected in series [−]
Nu	Nusselt number [−]
P	Power [W]
Pr	Prandtl number [−]
Ra	Rayleigh number [−]
S	Feed salinity [g/L]
T	Temperature [K] or [°C]
V	Volume [m^3]
vp	Position of the three-way mixing valve
w	Wind speed [m/s]

Greek symbols

α	Absorptivity [−]
β	Thermal coefficient for power [1/°C]
δ	Thickness [m]
ϵ	Emissivity [−]
η	Efficiency [−]
γ	Tuning parameter [m]
λ	Conductivity [W/(mK)]
μ_{hx}	Auxiliary factor [−]
ρ	Density [kg/m^3]
σ	Stefan-Boltzmann constant [W/(m^2K^4)]
τ	Transmissivity [−]
θ	Tilt angle of collectors [rad]
θ_{hx}	Auxiliary factor [−]

Subscripts and indices

a	Air
absh	Higher absorber
absl	Lower absorber
b	Back of collector
bes	Battery Energy System
el	Electric
f	Fluid
fw	Freshwater
g	Glass
gr	Ground
h	Heated seawater
hx	Heat Exchanger
in	Inlet
md	Membrane Distillation unit
n	Normalized
out	Outlet
p	Between the tank and the three-way valve
p,md	on the cold side of heat exchanger
p,t	on the hot side of heat exchanger
pumps	Pumps
pv	Photovoltaic
pvt	PV/T field
ref	Reference
s	Solar Thermal field
sf	Solar thermal fluid
sky	Sky
sw	Seawater or RO brine
t1	Upper side of Thermal Tank
t2	Bottom side of Thermal Tank
ted	Tedlar
TES	Thermal Energy Storage
th	Thermal

Acronyms

HX	Heat exchanger
KPIs	Key Performance Indicators
LCOW	Levelized Cost of Water [USD/m^3]
MD	Membrane Distillation
NOCT	Nominal Operating Cell Temperature [°C]
PC	Percentage of collector occupy by channel
PF	Packing Factor
PV	Photovoltaic
PVT	Photovoltaic Thermal
RO	Reverse Osmosis
RR	Recovery Ratio [−]
SEC	Specific Energy Consumption [kWh/m^3]
ST	Solar Thermal
V-AGMD	Vacuum Air Gap Membrane Distillation

1. Introduction

About half of the world's population experiences severe water scarcity for part of the year, and global water demand is projected to rise by 30% by 2050 [1,2]. Climate change and rising demand intensify pressure on freshwater resources. In Europe, despite a 19% reduction in water abstraction between 2000 and 2022, water scarcity affected about one-third of the EU territory and 41% of its population in 2022 [3].

1.1. Current status of desalination and related problems

Desalination of seawater and brackish water is increasingly adopted to meet domestic and municipal needs [4]. By 2022, more than 21,000 plants worldwide produced 99 million m^3/d of freshwater, with the MENA region accounting for 70% of global capacity [2]. In the EU, about 2178 plants supply 3.4 billion m^3/y, concentrated mainly in Spain, Greece, and Italy. In Spain, desalination covers only 2% of

national demand but is vital in regions such as Ceuta (88%) and Melilla (51%) [5]. For islands and isolated communities, desalination is often cheaper than water transport, which can exceed 10 €/m^3 [6].

There are several desalination technologies; the most widespread is Reverse Osmosis (RO) accounting for 68.7% of the global installed capacity, followed by Multi-Stage Flash (MSF) (17.6%), Multi Effect Distillation (MED) (6.9%), Nano Filtration (NF) (3.4%), Electro Dyalisis (ED) (2.4%), and other methods (1.0%) [7]. In the EU, the dominance of RO is even greater, representing 88.5% of total capacity [2].

RO is the most widespread technology thanks to its scalability, high efficiency (due to the use of electricity only) and lower cost of water compared to other technologies (0.45–1.72 USD/m^3) [7]. Its main drawback is the relatively high specific consumption of electrical energy (2.5–7 kWh/m^3) [8]. By contrast, alternative technologies require large amounts of thermal energy, which is generally less valuable than electricity.

The main challenge of desalination is brine disposal. Most plants discharge brine into the sea as the cheapest option [9], but this raises environmental concerns such as eutrophication, salinity increase, and toxicity, particularly in RO systems due to their high brine output [10,11]. Inland facilities cannot use marine discharge and instead rely on sewage systems, deep wells, evaporation ponds, or crystallizers, though all involve significant costs and environmental drawbacks [9].

1.2. Possible solutions to desalination problems

In order to address the problem of energy consumption of desalination, renewable energies can be employed to run the system, allowing the production of freshwater with minimal greenhouse gases emissions [11,12]. At the same time, desalination technology can be successfully exploited for demand response enhancing the grid power regulation flexibility and the penetration of renewable energies [13]. Regions with warm climates and greater water scarcity typically enjoy abundant solar radiation, making both photovoltaic and solar thermal ideal sources of renewable energy. In addition, the mismatch between renewable energy supply and demand, coupled with its intermittent availability, makes energy storage essential for maintaining the stable and uninterrupted operation of desalination plants [14,15].

Several authors have investigated the coupling of photovoltaic (PV) and solar thermal (ST) with desalination technologies.

Kettani et al. [16] have examined the cost competitiveness of a large-scale (2,75,000 m^3/d) solar-powered RO desalination plant in Morocco comparing different power supply configurations. They have found that the PV + grid is the cheapest power supply option with a cost of water equal to 0.98 USD/m^3.

Andrés-Mañas et al. [17] evaluated the annual performance of a vacuum multi-effect membrane distillation (V-MEMD) system powered by a solar thermal field with thermal storage using a quasi-dynamic model. They investigated a configuration where seawater is used to condense steam and preheat the feed. They found that a heat buffer in the desalination system stabilizes operation during solar radiation perturbations, and increasing the temperature setpoint boosts freshwater production.

Ehab M. Almetwally et al. [18] proposes a study that enhances a conical solar still by combining pistachio shells with paraffin-based PCM, which acts both as a solar absorber and an energy storage unit. Tested in Algeria, the hybrid design significantly boosted freshwater yield, efficiency, nighttime productivity, CO_2 mitigation, and economic viability, proving a low-cost and sustainable desalination solution for arid regions.

Regarding the environmental impact and disposal problems of the reject brine, it is worth of noting that it can be seen as a valuable resource rather than a waste [10], in fact in addition to being a source of freshwater, brine can also be a source of salts, minerals, metals, chemicals, bioactive compounds, and even energy [19,20]. To exploit the benefits of brine the concepts of Minimal Liquid Discharge (MLD) and Zero Liquid Discharge (ZLD) have been introduced [10].

Several approaches exist to achieve MLD or ZLD. A common method involves concentrating brine through multiple stages of desalination, resulting in very high water recovery. For example, brine from RO can be treated in a second-stage RO system, a Membrane Distillation (MD) unit, a forward osmosis (FO) unit, or a humidification-dehumidification (HDH) unit [9]. In addition, the use of crystallizers is very important in those context when aiming for a ZLD system, trying to completely eliminate liquid waste.

MD technology is a promising method for recovering water from brine produced by previous desalination modules because it requires low-grade heat (60–90 °C), which can be sourced from solar thermal systems or downstream of industrial processes.

Several authors have explored the integration of MD with RO. Mericq et al. [21] investigated an RO-vacuum membrane distillation (VMD) system through simulations and experiments, reporting a global recovery factor of 89%.

Son et al. [22] proposed a successful circular brine reclamation system combining RO, MD, and forward osmosis (FO) modules, enhancing crystallization efficiency in zero-liquid discharge applications.

Ngo et al. [23] evaluated the potential of the RO-MD system, achieving an overall water recovery rate of 98% with minimal membrane fouling.

1.3. The role of hybrid photovoltaic/Thermal collector in desalination

Since desalination systems require both thermal and electrical energy, Photovoltaic/Thermal (PV/T) technology is particularly appealing as it enables the simultaneous production of both [24,25]. Anand et al. [26] carried out a comparative analysis indicating that the overall performance of photovoltaic thermal (PV/T) coupled desalination systems surpasses that of desalination systems combined with separate photovoltaic panels and/or solar thermal collectors.

He et al. [8] highlighted the potential of the PV/T system to achieve higher solar utilization efficiencies, higher water production rates in electrically driven desalination processes, and lower lifetime water costs compared to PV desalination and solar thermal (ST) desalination systems. They also noted the limitations of PV/T technology, including its immaturity, system complexity, and high capital costs.

Numerous studies have investigated the integration of PV/T systems with desalination technologies, including configurations that combine multiple types of desalination units in hybrid systems. Wiesenfarth et al. [27] proposed a Concentrated Photovoltaic Thermal (CPV/T) system combined with RO and MD. Uche et al. [28,29] analyzed, through simulations and experiments, a small polygeneration unit powered by PV/T collectors, evacuated tube collectors, and a micro wind turbine. This system also enables drinking water production via an RO-MD setup with thermal storage. Li et al. [30] compared the energetic and exergetic performance of PV/T-RO-thermal distillation (TD) units with solar thermal distillation and PV-RO, finding the former to be more efficient. Mahmoudi et al. [31] developed a novel PV/T-powered MD desalination system and evaluated its performance under both indoor and dynamic outdoor conditions. Their results demonstrate that the fully integrated PV/T collector effectively provides the thermal and electrical energy necessary for the MD process. Ghazy et al. [32] present an annual performance analysis of a PV/T system integrated with adsorption desalination (ADS), evaluated under the climatic conditions of Sohag City, Egypt. The study demonstrates that the PV/T-ADS system outperforms conventional adsorption desalination technologies, indicating its potential to simultaneously mitigate energy and water scarcity in arid and semi-arid regions. Abdelgaied et al. [33] designed and constructed a hybrid desalination plant that achieves high productivity with low power consumption by integrating an RO unit with a conventional solar distiller. PV/T collectors and evacuated tube solar collectors were used to generate electricity and preheat the feed water. The results showed that this preheating approach enhanced water recovery and reduced energy use in the RO unit, although it led to a decrease in salt rejection.

Table 1
Comparison of our work with state of art solutions.

Reference	Methodology	Identified gap	Current work solution
[30]	Stationary simulation (point-specific design analysis)	Does not analyze dynamic solar variability or energy storage	Implements dynamic modeling with thermal and electrical storage
[31]	Field / Prototype (selected days in winter/summer)	Analyzes only MD; does not integrate RO or aim to improve RR through brine recovery	Proposes RO–MD coupling in series to maximize water recovery
[32]	Dynamic simulation (annual – 8760 hours)	Focuses on adsorption desalination; does not compare PV vs. PV/T systems	Compares System A (PV + ST) and System B (PV/T + ST) to improve efficiency
[33]	Field / Experimental (daily cycles of 8–10 hours)	Does not evaluate CO_2 savings or economic viability over a full annual cycle	Assesses CO_2 emissions and LCOW under annual operating conditions
[28,29]	Field / Pilot (long-term seasonal testing)	Focuses on domestic trigeneration; lacks specific attention to RR improvement	Prioritizes brine recovery to surpass conventional RO performance
[34]	Stationary simulation (project life cycle analysis)	Analysis limited to simple PV–RO; ignores the potential of PV/T hybrid technology	Shows that using PV/T reduces LCOW compared to traditional PV systems

1.4. Open challenges and contribution

The novelty of the work lies in the fact that it is the first to investigate the technical and economic performance of a desalination system designed to improve the recovery ratio using only solar energy, incorporating thermal energy storage and comparing the use of traditional photovoltaic panels with that of hybrid photovoltaic/thermal panels.

Unlike previous literature, this study introduces an RO configuration coupled with MD in series to maximize the value of brine. In addition, the study questions the use of static analysis by performing a dynamic simulation of the system over a year using real meteorological data from Almería (Spain). This assessment takes into account key performance indicators (KPIs) such as energy production, hybrid performance, economic viability, and the amount of CO_2 emissions saved.

In the context of the water-energy nexus, this work contributes in the following ways:

- Design reference: comparative analysis of PV and PV/T systems for minimum liquid discharge (RO + MD) desalination applications, which remains an experimental technology.
- Reference economic analysis: analysis of the LCOW in contrast to values in the literature, thereby validating the competitiveness of the hybrid solar system.
- Sustainability: quantitative determination of the capacity of these systems to operate using only renewable energy, thereby reducing their environmental impact and improving their RR.

Table 1 shows the gap identified in the literature and how this work contributes to it.

This article is divided into five sections. Section 2 describe the systems that are analyzed, Section 3 defines the method of the investigation, Section 4 proposed the results of the investigation and a discussion, and finally Section 5 presents the conclusions of our work.

2. Systems description

This article proposes and compares two desalination plants designed to produce freshwater while increasing the RR. The systems operate exclusively on solar energy, eliminating the need for reliance on the electricity grid or fossil fuels.

Each desalination plant consists of an RO system that generates freshwater using electrical energy stored in electrochemical batteries. The discharged brine is then processed by a set of vacuum air gap membrane distillation (V-AGMD) units. MD is a thermally driven process, in which the required thermal energy is stored in thermal storage tanks and transferred to the V-AGMD units via a pair of heat exchangers. To ensure complete treatment, the brine from the RO system is collected in a storage tank before MD. Then it is heated approximately to 80 °C using the aforementioned heat exchangers that transfer thermal energy from the fluid that circulates in the solar thermal field. A three-way valve, positioned between the thermal storage tanks and the heat exchanger, regulates the thermal energy supplied to the MD units. Energy storage systems enable freshwater production even in the absence of sunlight, such as at night. The RO process operates as long as there is sufficient energy in the battery system, while MD continues until there is enough thermal energy in the thermal storage tank and sufficient brine in the brine tank. Consequently, the RO and MD units do not function synchronously.

The two compared systems differ solely in their method of generating energy. The first system (System A) is powered by photovoltaic collectors and solar thermal collectors (PV-ST-RO-MD). The second (System B) utilizes hybrid flat plate photovoltaic/thermal and solar thermal collectors (PV/T-ST-RO-MD). In system B, the use of PV/T serves to increase electrical energy production by cooling the photovoltaic cells while simultaneously heating seawater to improve the RR of the RO unit.

The systems are assumed to be located in Almería, Spain, and are all designed to operate an RO unit with an inlet flow rate of 10 m^3/h. The operating time is proportional to the monthly in-plane solar irradiation, with a minimum in July of 8 hours of operation per day. Based on the average daily radiation data for Almería, obtained from PVGIS [35], the required photovoltaic system must have a peak electrical power of 18 kW for the PV and PV/T configurations.

The main characteristics of both systems are reported in Table 2,

Table 2
Main characteristics of systems A and B.

	System A	System B
Peak electrical power	18 kW	
N. of PV or PV/T collectors	36	42
N. of ST collectors	110	
Solar thermal panel	LBM 10 HTF	
N. of thermal storage tank	3	
Vol. of single thermal storage tank	18 m^3	
Vol. of brine tank	250 m^3	
Heat Exchanger	Sondex S14A-IG16-13-TL	
N. of Heat Exchanger	2	
Area of Heat Exchanger	1.65 m^2	
Heat transfer coefficient U	15,042	
RO inlet flow rate	10 m^3/h	
MD units	7	
MD inlet flow rate	1.1 m^3/h	
MD membrane area	25.92 m^2	
Battery capacity	11.7 kWh	
N. of batteries	4	

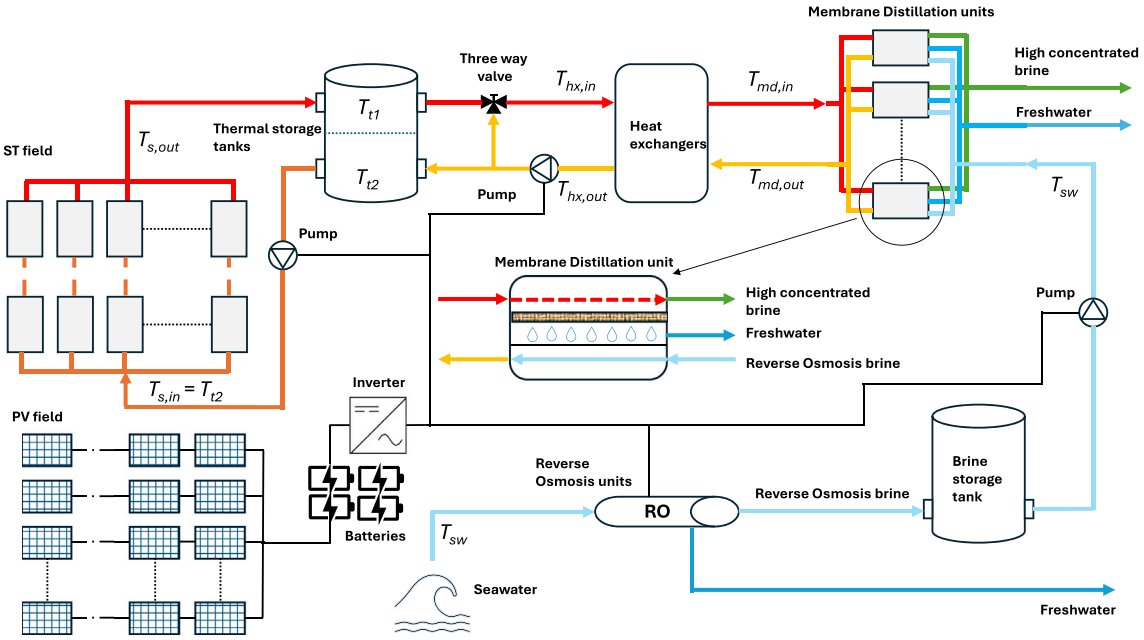

Fig. 1. Scheme of ST-RO-MD system (System A). The PV plant and battery system supply electricity to the pumps and RO unit. The resulting brine is stored in a tank and later processed by MD units. These MD units are powered by ST collectors via storage tanks and a heat exchanger, while the PV plant also provides electrical power for MD auxiliary components.

2.1. System A

The system is described by Fig. 1. The RO unit is powered by the photovoltaic plant and the MD units are powered by the solar thermal plant. The seawater is not preheated before entering the RO units.

2.1.1. Photovoltaic system

The main characteristics of the photovoltaic plant are reported in Table 3.

It is assumed that the slope angle of the solar collectors, both photovoltaic and thermal, is the optimal one i.e., 35 ° [35], and the azimuth angle is 0 °, meaning the panels are south-oriented.

In this analysis the effect of temperature on photovoltaic power production, P_{pv}, is considered, as reported in Eq. (1),

$$P_{pv} = I \cdot A_{pv} \cdot \eta_e, \tag{1}$$

where A_{pv} is photovoltaic area and I is the solar radiation intensity on the module plane [W/m^2] and η_e is the electric efficiency of the panel, that depends on cells temperature following Eq. (2),

$$\eta_e = \eta_{ref}\left[1 - \beta_{pv}\left(T_{pv} - T_{ref}\right)\right], \tag{2}$$

where η_{ref} is module efficiency at standard test condition (STC), β_{pv} is the thermal coefficient for power, T_{pv} is the temperature of the cells and T_{ref} is the reference temperature in Standard Test Condition (STC), i.e., 25°C.

The panel temperature is calculated starting from its normal operating cell temperature (NOCT), following the common expression:

$$T_{pv} = T_a + (NOCT - 20)\frac{I}{800}, \tag{3}$$

where NOCT is expressed in [°C].

Table 3
Main characteristics of the photovoltaic plant.

	System A
N. of panel	36
N. of string	2
Panel per string	18
Panel model	Q.PEAK DUO ML-G11S
Panel peak power	500 W
Temperature coefficient for power	−0.34%/°C
Cell efficiency at STC	21.1%
NOCT	43 °C
Area of panel	2.37 m^2

2.2. System B

The system is illustrated in Fig. 2. The substantial difference between this system and the previous one is the use of PV/T collectors instead of PV ones.

The RO unit, as well as all the other electrical loads, are powered by electricity generated by PV/T collectors equipped with an electrical storage system. Seawater is preheated by the PV/T to feed the RO with temperature higher than that of seawater in order to allow a lower electrical consumption and higher RR [36,37]. At the same time, seawater has the purpose of cooling the photovoltaic panel enhancing its efficiency. This allows the system to produce more electricity and therefore to treat more water.

The temperature at the inlet of RO is maintained lower than 30 °C, by means of a three-way valve that mixes cold seawater with the preheated seawater at the outlet of PV/T, in order to maintain acceptable permeate quality, since salt concentration in permeate increase with temperature [37], avoid fouling problem, which increases with temperature [38] and reduce the electric consumption, since it starts to increase with temperature when it is greater than 30 °C [37]. In any case, the flow rate at the inlet of RO is maintained constant and equal to 10 m^3/h.

Preheating water for RO can improve its efficiency, but it may reduce the productivity of MD units [39]. This is because the cooling brine, at a higher temperature, has a lower condensing capacity. However, the increased temperature of the brine reduces the thermal power required from the solar thermal field, extending the system's operating hours. Therefore, the aim of our study is also to assess the productivity of this desalination system considering these two contrasting effect.

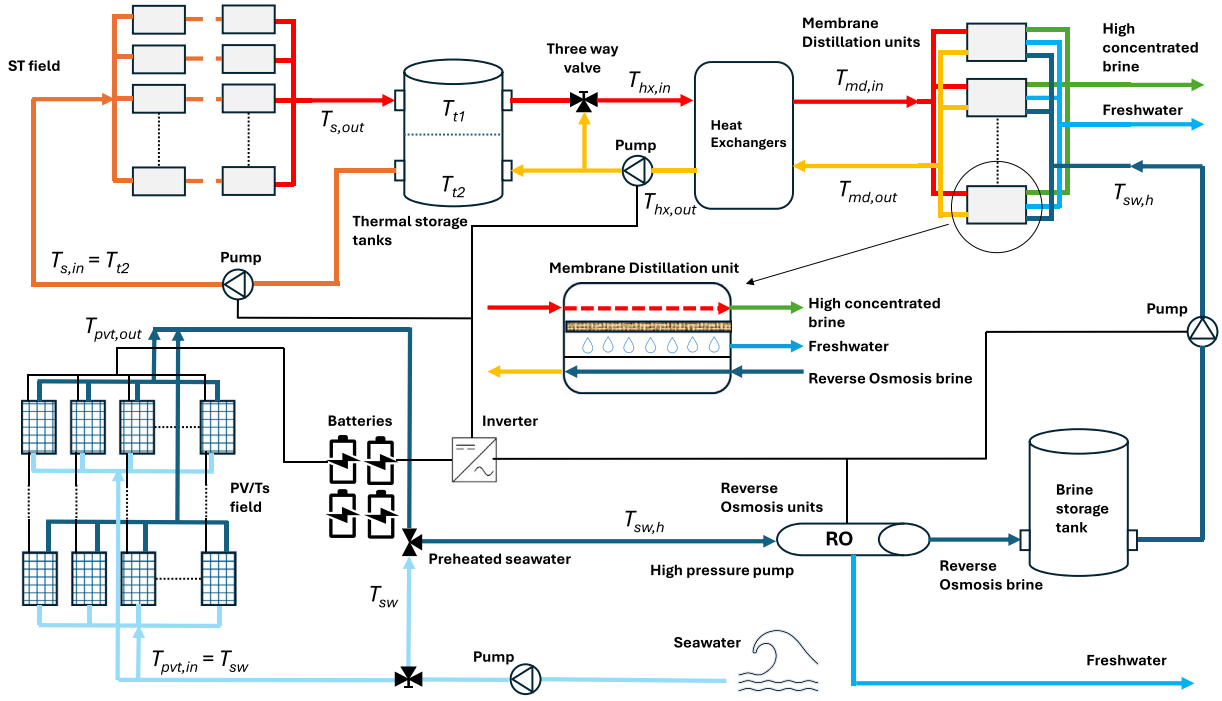

Fig. 2. Scheme of PV/T-ST-RO-MD system (System B). The PV/T plant and battery system supply electricity to the pumps and RO unit, furthermore it increases the temperature of seawater enhancing the RR of RO unit. The brine produced is stored in a tank and later processed by MD units. These MD units are powered by ST collectors via storage tanks and a heat exchanger, while the PV/T plant also provides electrical power for MD auxiliary components.

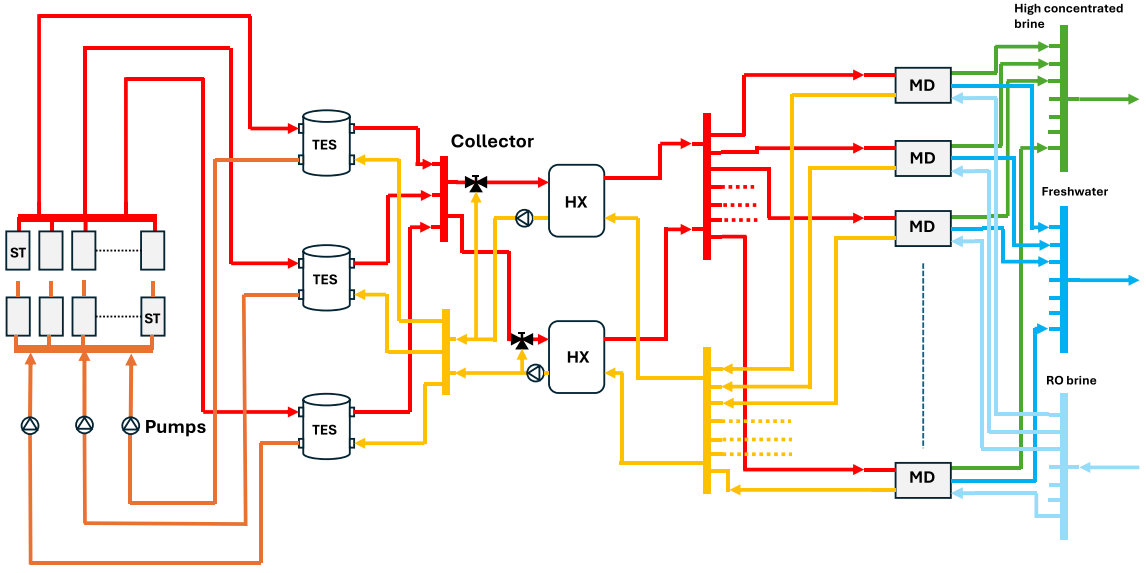

Fig. 3. Detailed representation of the thermal connections between solar thermal panels (ST), thermal storage tanks (TES), heat exchangers (HX) and MD units. The arrows indicate the direction of the water flow.

The thermal power supply of the MD system is shown in a simplified form in Figs. 1 and 2 for conciseness. A more detailed representation of the thermal connections is provided in Fig. 3, offering clearer insight into this aspect.

2.2.1. PV/T system

The PV/T solar thermal field consists of 42 parallel-thermally connected collectors. These collector are electrically connected considering 2 strings of 21-series connected panels. Even in this case it is assumed that the slope angle, θ, of the solar collectors is the optimal one (35 °) as well as the azimuth angle (0 °) [35].

The PV/T system model considered in this study is the one-dimensional one presented by C. El Fouas et al. [40]. The PV/T panel is considered as a multi-layer system. Each PV/T panel is composed by six layers: the first is the frontal glass, which follows photovoltaic cells, Tedlar layer, higher absorber, fluid (water) and lower absorber layer. The model is based on energy balance equations of each layer [40].

- Energy balance equation of glass:

$$\varrho_g \delta_g c_g \frac{dT_g}{dt} = \alpha_g I + hr_{g,sky}\left(T_{sky} - T_g\right) + hr_{g,gr}\left(T_{gr} - T_g\right) + hv_{g,a}\left(T_a - T_g\right) + hc_{pv,g} PF \left(T_{pv} - T_g\right) + hc_{ted,g}\left(1 - PF\right)\left(T_{ted} - T_g\right), \quad (4)$$

where T_g, T_{sky} and T_{gr} are the glass, sky and ground temperature in [K], respectively; I is the solar radiation, in [W/m^2], on the plane of the array. The coefficients $hr_{g,sky}$, $hr_{g,gr}$ are the radiative heat transfer coefficient between glass and sky and between glass and ground respectively; $hv_{g,a}$ is the convective heat transfer coefficient between glass, while $hc_{pv,g}$ and $hc_{ted,g}$ are conductive heat transfer coefficient between glass and photovoltaic cells and Tedlar layer respectively. Each heat transfer coefficient is calculated in [W/(m^2°C)]. The notation hr always indicate a radiative heat transfer coefficient, while the notation hv and hc indicate the convective and conductive heat transfer coefficient respectively.
The radiative heat transfer coefficient between glass and sky and between glass and ground are calculated as follows:

$$hr_{g,sky} = \sigma \varepsilon_g F_{g,sky}\left(T_{sky} + T_g\right)\left(T_{sky}^2 + T_g^2\right), \quad (5)$$

$$hr_{g,gr} = \sigma \varepsilon_g F_{g,gr}\left(T_{gr} + T_g\right)\left(T_{gr}^2 + T_g^2\right), \quad (6)$$

where, σ is the Stefan-Boltzmann constant and the view factors, $F_{g,sky}$ and $F_{g,gr}$, are calculated as follows:

$$F_{g,sky} = \frac{1 + \cos\theta}{2}, \quad (7)$$

$$F_{g,gr} = \frac{1 - \cos\theta}{2}. \quad (8)$$

The convection coefficient depends on the convection regime. It can be forced, natural or mixed [40–42].

$$hv_{g,a} = \begin{cases} 5.7w + 11.4 & \text{for forced convection} \\ \frac{Nu_{free}\lambda_a}{L} & \text{for free convection} \\ \left(hv_{forced}^3 + hv_{free}^3\right)^{1/3} & \text{for mixed convection} \end{cases}$$

where w is wind speed, Nu_{free} is the Nusselt number and λ_a is the conductivity of air.
The conductive heat transfer coefficient is calculated according to the following equation:

$$\frac{1}{\frac{\delta_g}{2\lambda_g} + \frac{\delta_{pv}}{2\lambda_{pv}}}. \quad (9)$$

The following conductive heat transfer coefficients are calculated according to the same expression of Eq. (9), obviously considering the conductivity and thickness of the layers taken into account.

- Energy balance equation of PV cells:

$$PF\left(\varrho_{pv}\delta_{pv}c_{pv}\right)\frac{dT_{pv}}{dt} = PF\left[\left(\tau_g\alpha_{pv} - \eta_e\right)I\right] + PF\left[hc_{pv,g}\left(T_g - T_{pv}\right) + hc_{ted,pv}\left(T_{ted} - T_{pv}\right)\right], \quad (10)$$

where T_{pv} is temperature of the cell, PF is the packing factor i.e., ratio between the surface covered by the PV cells and the total surface of the PV/T panel, η_e is calculated according to Eq. (2), and electric power from PV/T is calculated following the Eq. (1).

- Energy balance equation of Tedlar:

$$\rho_{ted}\delta_{ted}c_{ted}\frac{dT_{ted}}{dt} = \left(1 - PF\right)\tau_g\alpha_{ted}I + \left(1 - PF\right)hc_{ted,g}\left(T_g - T_{ted}\right) + PFhc_{ted,pv}\left(T_{pv} - T_{ted}\right) + hc_{absh,ted}\left(T_{absh} - T_{ted}\right) \quad (11)$$

- Energy balance equation of upper absorber layer:

$$\rho_{absh}\delta_{absh}c_{absh}\frac{dT_{absh}}{dt} = hc_{absh,ted}\left(T_{ted} - T_{absh}\right) + \left(1 - PC\right)hc_{absl,absh}\left(T_{absl} - T_{absh}\right) + PChr_{absl,absh}\left(T_{absl} - T_{absh}\right) + hc_{f,absh}\left(T_f - T_{absh}\right), \quad (12)$$

where T_{absh} indicates the temperature of the upper absorber layer and PC represents the percentage of channel i.e., the ratio between the surface area where the fluid flows and the total surface area of the panel.
The radiative heat transfer coefficient $hr_{absl,absh}$ between the two absorber plates, made of aluminum, is calculated following the equation [40,43]:

$$hr_{absl,absh} = \frac{4\sigma\bar{T}^3}{\left(\frac{1}{\varepsilon_{abs}} + \frac{1}{\varepsilon_{abs}} - 1\right)}, \quad (13)$$

where, $\bar{T}$ is the absorbers mean temperature.

- Energy balance equation of lower absorber layer:

$$\rho_{absl}\delta_{absl}c_{absl}\frac{dT_{absl}}{dt} = hc_{absl,f}(T_f - T_{absl}) + (1 - PC)hc_{absl,absh}(T_{absh} - T_{absl}) + PChr_{absl,absh}(T_{absh} - T_{absl}) + hv_{a,absl}(T_a - T_{absl}) + hr_{sky,absl}(T_{sky} - T_{absl}) + hr_{gr,absl}(T_{gr} - T_{absl}), \quad (14)$$

where, T_{absl} indicates the temperature of the lower absorber layer. The convective heat transfer coefficient between the lower absorber and the ambient air is determined depending on the convection regime. In free convection, the Nusselt number is calculated as follows [40,44]:

$$Nu_{free} = \left\{0.825 + \frac{0.387Ra^{1/6}}{\left[1 + \left(\frac{0.492}{Pr}\right)^{9/16}\right]^{8/27}}\right\}^2, \quad (15)$$

while in forced convection the coefficient is expressed by [40]:

$$hv_{a,absl} = 5.7w_b, \quad (16)$$

in which w_b is the wind speed at the back of collector.

- Energy balance equation of heat transfer fluid:

$$\rho_f\delta_f c_f\frac{dT_f}{dt} = hc_{f,absh}\left(T_{absh} - T_f\right) + hc_{absl,f}\left(T_{absl} - T_f\right) - \dot{m}_f C_f\left(T_{out} - T_{in}\right), \quad (17)$$

Table 4
Main characteristics of photovoltaic/thermal plant.

	System B
N. of panels	42
N. of strings	2
Panels per string	21
Panel model	DualSun SPRING4 425 TOPCon Finned
Panel peak power	425 W
Temperature coefficient for power	−0.31%/°C
Cell efficiency at STC	21.8%
Area of panel	1.95 m^2

Table 5
Main characteristics of the PV/T panel.

Layer	Symbol	Parameter	Value
Glazing	A	Aperture area [m^2]	1.95
	L_g	Length [m]	1.722
	W_g	Width [m]	1.134
	δ_g	Thickness [m]	0.003
	c_g	Specific heat [kJ/(kg·K)]	0.500
	ρ_g	Density [kg/m^3]	2300
	λ_g	Thermal conductivity [W/(m·K)]	1.0
	α_g	Absorptivity [−]	0.03
	τ_g	Transmittance [−]	0.92
	ϵ_g	Emissivity [−]	0.95
PV cells	PF	Packing Factor [−]	0.88
	δ_{pv}	Thickness [m]	0.00035
	c_{pv}	Specific heat [kJ/(kg·K)]	0.757
	ρ_{pv}	Density [kg/m^3]	2330
	λ_{pv}	Thermal conductivity [W/(m·K)]	168.0
	α_{pv}	Absorptivity [−]	0.93
	η_{ref}	Electrical efficiency at STC [%]	21.8
Tedlar	δ_{ted}	Thickness [m]	0.0002
	c_{ted}	Specific heat [kJ/(kg·K)]	1.200
	ρ_{ted}	Density [kg/m^3]	1500
	λ_{ted}	Thermal conductivity [W/(m·K)]	0.2
	α_{ted}	Absorptivity [−]	0.90
Channel fluid	PC	Percentage of the Channel [−]	0.67
	δ_f	Thickness [m]	0.0015
	c_f	Specific heat [kJ/(kg·K]	4.168
	ρ_f	Density [kg/m^3]	997
	λ_f	Thermal conductivity [W/(m·K)]	0.606
Absorber plate	δ_{abs}	Thickness [m]	0.001
	c_{abs}	Specific heat [kJ/(kg·K)]	900
	λ_{abs}	Thermal conductivity [W/(m·K)]	160
	ϵ_{abs}	Emissivity [−]	0.4

where $\dot{m}_f$ is the mass flow rate of the fluid, in [kg/s]. Its value depends on the three-way valve aperture; when it is completely open the flow rate is equal to the ratio between the RO feed water flow rate and the number of PV/T collectors, i.e., 0.238 m^3/h, that in terms of mass flow rate depends on seawater density and is approximately equal to 0.068 kg/s. The fluid temperature T_f is calculated as:

$$T_f = \frac{T_{pvt,out} + T_{pvt,in}}{2} \tag{18}$$

where $T_{pvt,out}$ is the fluid temperature at the outlet of the panel and $T_{pvt,in}$ is the fluid temperature at the inlet of the panel, equal to seawater temperature T_{sw}.

The method for calculating the coefficients in the energy balance equations is described in [40]. In our work, the thermal properties of the PV/T panel are consistent with those reported by [40]. However, for the electrical and geometrical characteristics, such as the panel area, we referred to the specifications of the DualSun SPRING4 425 TOPCon Finned model [45]. The main features of the PV/T plant, along with the panel's electrical properties, are presented in Table 4. The main thermal and geometrical properties of each layer of the panel are provided in [40] and in Table 5. Additionally, [40] presents the thermal circuit and a graphical representation of the PV/T panel.

2.3. Desalination system

In every system, the MD unit (from the Dutch company Aquastill) is a vacuum-assisted air gap type (V-AGMD), meaning that air is sucked from the gap. This V-AGMD unit allows the condensation of water vapor inside the module by exchanging the latent heat of condensation with the brine coming from the RO unit, which simultaneously preheats the brine, enabling energy recovery.

2.3.1. Reverse osmosis unit

This study considers an RO system equipped with an energy recovery device (ERD) and a fixed input flow rate of 10 m^3/h. Based on this flow rate and the requirement for a minimum of 8 hours of operation in July, the entire system is designed accordingly.

Rather than focusing on a specific commercial RO unit, the system's performance is derived from prior characterization studies [36,37]. The analysis examines how RO performance, expressed as Recovery Ratio (RR) and Specific Electric Consumption (SEC), varies with seawater temperature considering constant feed water pressure and constant salinity, fixed at 40 mg/l. The relationship between RR and seawater temperature is derived from the data presented in Table 6, based on the table reported by [36]. This analysis assumes a feed pressure of 54 bar and a seawater salinity of 40 mg/L. The relationship between these data is expressed by Eq. (19)

$$RR = 0.0083 \cdot T_{sw} + 0.2472, \tag{19}$$

where T_{sw} is seawater temperature.

The relationship between Specific Electric Consumption (SEC), defined as the electrical energy required per unit of permeate produced, and seawater temperature is provided by [37] for a feed salinity of 40 mg/L, as shown in Table 7. The relationship is described by a quadratic equation, as reported by Eq. (20)

$$SEC = 0.0007 \cdot T_{sw}^2 - 0.0444 \cdot T_{sw} + 3.0616. \tag{20}$$

Eq. (20) shows that specific consumption increases once the temperature exceeds approximately 30 °C. Mohammadi et al. [38] demonstrated that fouling increases linearly with temperature, while permeate flux also improves, with an optimal feed temperature of 35 °C. However, scaling also worsens at higher temperatures. Therefore, in the operation of System B, the RO feed temperature is kept below the 30 °C threshold.

2.3.2. Membrane distillation units

The MD units under consideration operate using a vacuum-assisted air gap configuration. The equations describing the behavior of a single module are based on the work of Andrés-Mañas et al. [39], who characterized a real MD unit using Response Surface Methodology. The module is referred to as AS26, since its membrane area is approximately equal to 26 m^2.

Table 6
Seawater temperature and RR according to [36] for a feed pressure equal to 54 bar and seawater salinity equal to 40 mg/l.

Temperature [°C]	20	25	30	35	40	45
RR	0.415	0.455	0.496	0.539	0.581	0.623

Table 7
Seawater temperature and Specific Electricity Consumption according to [37] for seawater salinity equal to 40 mg/l.

Temperature [°C]	15	20	25	30	35	40
SEC [kWh/m^3]	2.550	2.450	2.376	2.350	2.352	2.384

Table 8
Normalization coefficient reported by [39].

Coefficient	$T_{md,in,n}$	$F_{feed,n}$	$T_{sw,n}$	$S_{feed,n}$
k_0	−7	−2.1429	−5	−1.3333
k_1	0.1	0.0029	0.2	0.0095

The equations derived by the authors describe the relationship between the permeate flux J, [$Lh^{-1}m^{-2}$], and several normalized input variables: the heated seawater temperature at the inlet of the evaporation channel $T_{md,in,n}$, the feed flow rate, $F_{feed,n}$, the feed salinity, $S_{feed,n}$, and the seawater temperature at the inlet of the feed channel, $T_{sw,n}$. Additionally, the equations characterize the relationship between the temperature of the seawater pre-heated within the MD unit, $T_{md,out}$, and the same set of normalized variables.

$$\begin{aligned} J = {} & 0.80 + 0.32 \cdot T_{md,in,n} + 0.56 \cdot F_{feed,n} - 0.15 \cdot T_{sw,n} \\ & - 0.66 \cdot S_{feed,n} + 0.19 \cdot T_{md,in,n} \cdot F_{feed,n} \\ & - 0.11 \cdot T_{md,in,n} \cdot S_{feed,n} - 0.19 \cdot F_{feed,n} \cdot S_{feed,n}, \end{aligned} \tag{21}$$

$$\begin{aligned} T_{md,out} = {} & 65.11 + 9.16 \cdot T_{md,in,n} - 0.92 \cdot F_{feed,n} \\ & + 0.48 \cdot T_{sw,n} - 1.06 \cdot S_{feed,n} \\ & + 0.15 \cdot T_{sw,n} \cdot F_{feed,n}. \end{aligned} \tag{22}$$

Normalization is a procedure of transforming the value of a variable in a dimensionless value between −1 and +1. The normalization is carried out following the procedure described by [39]. Generally normalization of a generic variable x follows the expression:

$$x_n = \frac{2\left(x - x_{min}\right)}{x_{max} - x_{min}} - 1 \tag{23}$$

This formula can be rewritten following a linear expression considering the maximum and minimum value of each variable.

$$x_n = k_0 + k_1 x, \tag{24}$$

where k_0 and k_1 are coefficient derived from Eq. (23). The way of obtaining that coefficient is reported by [39] and their value is also reported in Table 8.

According to Table 2, the MD system comprises 7 units. This configuration was designed to ensure that the system can process the entire volume of brine discharged by the RO units, thereby preventing overload of the brine storage tank.

2.4. Solar thermal units

Solar thermal system considered consist of n_p panels connected in parallel to form a collector and n_s collectors connected in series to form a so-called loop. The solar thermal system consist of n_l loops. The characteristics of panel and of the solar thermal system are reported in Table 9. The solar thermal system was sized based on the most unfavorable month of the year, i.e., the month with the lowest solar radiation, to ensure that the MD units can continue operating even under those conditions.

The equation governing a solar thermal loop are derived by Andrés-Mañas et al., [17] and reported below:

$$\begin{aligned} \rho_{sf} \cdot c_{sf} \cdot A_s \cdot \frac{dT_{sf,out}(t)}{dt} = {} & \gamma \cdot I(t) - \frac{H \cdot (T_{sf,out}(t) \cdot 0.5 + T_{sf,in}(t) \cdot 0.5 - T_a(t))}{L \cdot n_s} \\ & - \frac{Cp_{sf} \cdot \dot{m}_s \cdot (T_{s,out}(t) - T_{s,in}(t))}{L \cdot n_s \cdot n_p \cdot n_a}, \end{aligned} \tag{25}$$

where, ρ_{sf} is the density of the solar thermal fluid (pressurized water), in [kg/m^3], C_{sf} is its the specific heat, in [J/(kg°C)], A_s is the cross-section area of the panel pipe, γ is a tuning parameter that modulates the solar irradiance collection, in [m], I is the solar irradiance on the plane of collector in [W/m^2], H is thermal losses coefficient in [J/(s°C)], L represents the flat plate tube length, in [m], T_a is ambient temperature, in [°C], $T_{sf,out}$ and $T_{sf,in}$ are the outlet and inlet temperature of solar thermal loop, in [°C], respectively, m_s the mass flow rate of fluid which runs through the solar loop, in [kg/s] and finally n_a and L are the number of tubes in each flat plate collector and their length, in [m], respectively.

Table 9
Solar thermal system characteristics.

A_s	$2.8 \cdot 10^{-5}$ m^2
H	5.88 J/(s°C)
L	1.15 m
n_a	20
n_p	5
n_s	5
n_l	22
β	0.11 m
$\dot{m}_s$	0.25 kg/s

2.5. Thermal storage tank

The thermal energy storage tank (TES) stores thermal energy by means of heated water and is modeled using the equations presented by Andrés-Mañas et al. [17]. The tank is divided into two sections, with an energy balance applied to each section individually.

$$\begin{aligned} \frac{\rho_f \cdot V_{TES}}{2} \cdot \frac{dT_{t1}}{dt} = {} & f_a \cdot \dot{m}_s \cdot (T_{sf,out} - T_{t1}) + f_b \cdot \dot{m}_p \cdot (1 - vp) \cdot (T_{t2} - T_{t1}) \\ & - \frac{UA_1 \cdot (T_{t1} - T_{amb})}{c_{p,f}}, \end{aligned} \tag{26}$$

$$\begin{aligned} \frac{\rho_f \cdot V_{TES}}{2} \cdot \frac{dT_{t2}}{dt} = {} & f_a \cdot \dot{m}_{sf} \cdot (T_{t1} - T_{t2}) + f_b \cdot \dot{m}_p \cdot (1 - vp) \cdot (T_{hx,out} - T_{t2}) \\ & - \frac{UA_2 \cdot (T_{t2} - T_{amb})}{c_{p,f}}. \end{aligned} \tag{27}$$

Where V_{TES} is the volume of the thermal energy storage tank ($18\,m^2$); $\dot{m}_s$ and $\dot{m}_p$ are the mass flow rates from the solar collectors to the tank, and from the three-way valve to the heat exchangers if the valve does not allow fluid recirculation, respectively. $T_{s,out}$ is the outlet temperature of the fluid from the solar collectors. T_{t1} and T_{t2} represent the temperatures at the top and bottom of the tank, respectively. UA_1 and UA_2 are the thermal loss coefficients, equal to 3.7 W/°C, at the top and bottom of the tank, respectively. vp denotes the position of the three-way mixing valve between the heat storage tank and the heat exchanger, where 1 indicates full circulation and 0 indicates no recirculation.

The equations reported by [17] have been modified adding the two factors f_a and f_b. Their purpose is taking into account the number of MD units, ST loops and TES considered in the system.

$$f_a = \frac{n_l}{n_{TES}}, \quad f_b = \frac{n_{MD}}{n_{TES}}. \tag{28}$$

In fact, $\dot{m}_s$ is the flow rate in a single loop of solar thermal field; in order to consider the feed flow rate in a single TES the number of units has to be considered, therefore the factor a. The same concept applies to factor b: $\dot{m}_p$ is the mass flow rate, equal to 0.42 kg/s, related to heat exchanger in a system in which only a single MD unit and a single TES unit are considered. In order to consider the presence of multiple MD and TES units, factor b is needed.

The number and capacity of the thermal storage tanks were determined based on the sizing of the solar thermal collectors, specifically considering the most unfavorable day of the year—i.e., the day with the lowest solar radiation—to ensure that the MD units can continue operating even under such conditions. Finally, following this same design paradigm, the heat exchangers were also sized accordingly.

2.6. Heat exchangers

The heat exchanger model is proposed by Gil et al. [46]. The outlet temperature on the hot side of the heat exchanger, $T_{hx,out}$, and the outlet temperature on the cold side of the heat exchanger, i.e., the temperature of RO brine at the inlet of the hot side of the MD unit, $T_{md,in}$, are calculated using Eqs. (29) and (30):

$$T_{hx,out} = T_{hx,in} - \mu_{hx,1} \cdot (T_{hx,in} - T_{md,out}), \tag{29}$$

$$T_{md,in} = T_{md,out} + \mu_{hx,2} \cdot (T_{hx,in} - T_{hx,out}), \tag{30}$$

where, $T_{hx,in}$ is the input temperature at the hot side of the heat exchanger and $\mu_{hx,2}$, $\mu_{hx,1}$ and θ_{hx} are auxiliary factors calculated as follows:

$$\mu_{hx,2} = \frac{f_c \cdot \dot{m}_t \cdot c_{p,t}}{f_c \cdot \dot{m}_{md} \cdot c_{p,md}}, \tag{31}$$

$$\mu_{hx,1} = \frac{1 - e^{\theta_{hx}}}{1 - \mu_{hx,2} \cdot e^{\theta_{hx}}}. \tag{32}$$

$$\theta_{hx} = U_{hx} A_{hx} \cdot \left(\frac{1}{f_c \cdot \dot{m}_t \cdot c_{p,t}} - \frac{1}{f_c \cdot \dot{m}_{md} \cdot c_{p,md}} \right), \tag{33}$$

where $\dot{m}_t$ and $c_{p,t}$ are the mass flow rate and specific heat capacity of the fluid on the hot side of the heat exchanger, while $\dot{m}_{md}$ and $c_{p,md}$ refer to the cold side of the heat exchanger, i.e., the fluid at the inlet of the MD evaporation channel. U_{hx} [W/m^2°C] and A_{hx} [m^2] represent the heat transfer coefficient and the surface area of the heat exchanger, respectively, and are equal to 15,042 W/m^2°C and 1.65 m^2. The factor f_c has the same conceptual meaning as the previous factors and is defined as:

$$f_c = \frac{n_{MD}}{n_{HX}}, \tag{34}$$

where n_{HX} is the number of heat exchangers.

2.7. Battery energy system

The battery energy storage system consists of 4 batteries with 11.7 kWh capacity, as reported in Table 2. The selected technology is Li-ion, chosen for its long lifespan. The battery system was sized based on the month of July, i.e., the period with the highest freshwater production demand. We calculated the equivalent sun hours and, consequently, the daily energy required by the system in the absence of standard solar radiation. Considering this energy demand, a battery depth of discharge of 80% and a storage efficiency of 90% were applied to determine the required storage capacity. The number of batteries was then obtained by dividing the daily energy to be stored by the capacity of a commercial unit (LG Enblock C12).

The equation that describes the energy stored in the battery system, E_{bes} is the following:

$$\frac{dE_{bes}}{dt} = P_{pv} - P_{RO} - P_{MD} - P_{pumps}, \tag{35}$$

where P_{pv} is the electrical power produced by PV or PV/T panel, and P_{RO}, P_{MD} and P_{pumps} are the electrical powers consumed by RO, MD and pumping system respectively.

3. Evaluation methodology

This section describes the approach adopted to assess the performance of the two desalination systems. The performance is evaluated in terms of economic index, namely Levelized Cost of Water (LCOW), in terms of water production, RR and amount of yearly CO_2 gas emission avoided.

Table 10
Seawater temperature [°C] in Almería by month. Values are calculated based on the data over the past 10 years.

Month	Min	Max	Average
January	13.4	17.3	15.2
February	13.4	16.7	14.8
March	13.6	16.7	15.0
April	13.6	18.8	16.0
May	14.8	20.8	18.1
June	16.2	24.5	20.6
July	18.2	27.8	23.8
August	21.4	28.1	25.3
September	20.0	27.5	23.8
October	15.4	24.0	21.2
November	14.7	21.6	18.1
December	14.2	18.8	16.4

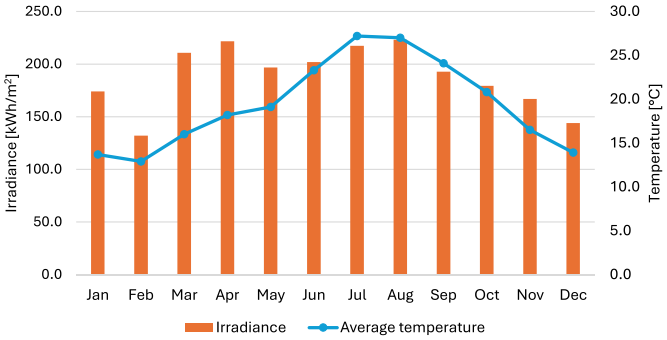

Fig. 4. Monthly irradiation [kWh/m^2] on optimal inclined plane and monthly average temperature in Almería.

3.1. Location

It is assumed that both systems are located in Almería (Spain), situated on the Mediterranean coast and characterized by a hot, arid climate with an average annual temperature equal to 18.43 °C, global annual solar radiation on a horizontal plane equal to 1859.59 kWh/m^2 [35] and average seawater temperature between 14.8 °C and 25.3 °C [47]. Weather data of Almería are taken from PVgis [35], while the seawater temperature data are taken from [47] and are reported in Table 10. Monthly optimal irradiation on an optimal inclined plane and monthly average ambient temperature are reported in Fig. 4 [35].

Seawater temperature plays a crucial role in determining the outlet water temperature of the PV/T panels. Specifically, during warmer months, when seawater temperature is high, a three-way valve installed upstream of the PV/T panels diverts part of the flow directly to the RO unit. This mechanism prevents the inlet temperature of the RO unit from exceeding 30 °C. In our study, we used the average seawater temperature for each month of the year.

3.2. Operation mode

The desalination systems operate based on the availability of thermal and electrical energy, as well as the volume of brine in the tank. Therefore, we considered multiple operating modes. In our work, we enhanced and implemented the MD desalination control logic proposed by [17], incorporating the availability of electrical energy, thermal energy, and water in the brine tank.

Regarding the MD desalination system, 4 operation modes exist:

- **Mode 0**: Stop mode, all units (ST and MD) are off and no distillate is produced.
- **Mode 1**: The ST units are off due to low irradiance, but the MD units run using stored heat.

- **Mode 2**: Solar fluid heats the storage system, but not enough to run the MD unit. The ST system is on; the MD units are off.
- **Mode 3**: The MD unit runs while solar fluid heats the storage system. Both ST and MD units are active.

Regarding the RO desalination unit, only 2 operation modes are considered:

- **Mode 0**: Stop mode. RO pump is off and no flow circulates through the PV/T system.
- **Mode 1**: RO unit runs and a seawater flow rate circulates through the PV/T system.

The control logic of operation mode is described by the Algorithm 1.

The index k indicates the time instant at which the calculation is obtained and SOC_{BAT_k} is the State of Charge of batteries.

The control of the three-way valve position between the thermal storage tanks and the heat exchangers is obtained by means of Algorithm 2.

Finally, there is no algorithm that directly controls the position of the PV/T three-way valve. Instead, an algorithm has been implemented to calculate the flow rate within the PV/T system, as shown in Algorithm 3.

In this algorithm, $\dot{V}_{RO}$ is the volumetric flow rate of seawater at the inlet of the RO unit, while ρ_{sw} is the seawater density and n_{PVT} is the number of PV/T panels. The mass flow rate in PV/T panels is forced to always be higher than 0.03 kg/s to avoid overheating of the fluid. This algorithm allows to obtain seawater temperature always lower than or equal to 30 °C.

3.3. Economic analysis

To assess and compare the economic viability of the systems, the LCOW is computed through an analysis of all associated expenditures. Each element of the system is priced using either current market valuations or specific literature references. The LCOW is defined as the ratio between the system's total net annual cost and the total volume of water produced over one year.

The total annual cost comprises the sum of annualized capital expenditures, C_1, yearly operation and maintenance costs, C_2 as well as RO and MD membrane replacement costs, C_3 and C_4 respectively. Therefore the LCOW is calculated as reported in Eq. (36)

$$LCOW = \frac{\sum_{j=1}^{4} C_j}{V_{fw}}, \tag{36}$$

where V_{fw} is total volume of water yearly produced.

The annualized capital cost, C_1 is calculated by multiplying the total capital cost, C_{cap} by the amortization factor a, given by the following expression:

$$a = \frac{k(1+k)^N}{(1+k)^N - 1}, \tag{37}$$

where k is the annual interest rate and N is the system lifetime; these values are reported in Table 12.

Each cost of the systems is reported in Table 11. Costs are reported in USD; however, some sources provided costs in Euros. To convert these to USD, we multiplied the Euro amounts by a factor of 1.1. The characteristics of the system, i.e., the size of the components and their number, are shown in Tables 2–4. The procedure to calculate the total annual cost of the systems is reported in Table 12.

3.4. Environmental analysis

Environmental analysis involves calculating the amount of carbon dioxide, CO_2, that each system prevents from being emitted into the atmosphere during water production.

Algorithm 1 Logic of operation of RO and MD systems.

if $SOC_{BAT_k} > 15$ **then**
  $mode_{ro_k} \leftarrow 1$
  $E_1 \leftarrow \begin{cases} 1 & \text{if } I_k > 500\,W/m^2 \text{ and } T_{sout_k} < 100\,°C \\ 0 & \text{otherwise} \end{cases}$
  $E_2 \leftarrow \begin{cases} 1 & \text{if } I_k \leq 500\,W/m^2 \text{ or } T_{sout_k} > 115\,°C \text{ or} \\ & (T_{sout_k} < T_{t1_k} \text{ and } mode_{md_k} = 3) \\ 0 & \text{otherwise} \end{cases}$
  $E_3 \leftarrow \begin{cases} 1 & \text{if } T_{t1_k} > 80\,°C + 1 \\ 0 & \text{otherwise} \end{cases}$
  $E_4 \leftarrow \begin{cases} 1 & \text{if } T_{t1_k} < 80\,°C \\ 0 & \text{otherwise} \end{cases}$
  $E_5 \leftarrow \begin{cases} 1 & \text{if } V_{Brine\_tank_k} \leq 10\,m^3 \\ 0 & \text{otherwise} \end{cases}$
  $E_6 \leftarrow \begin{cases} 1 & \text{if } V_{Brine\_tank_k} > 50\,m^3 \\ 0 & \text{otherwise} \end{cases}$
  if $mode_{md_{k-1}} = 0$ **then**
    if $E_1 = 0$ and $E_3 = 1$ and $E_6 = 1$ **then**
      $mode_{md_k} \leftarrow 1$
    else if $E_1 = 1$ and $E_3 = 0$ **then**
      $mode_{md_k} \leftarrow 2$
    else if $E_1 = 1$ and $E_3 = 1$ and $E_6 = 1$ **then**
      $mode_{md_k} \leftarrow 3$
    else
      $mode_{md_k} \leftarrow mode_{md_{k-1}}$
    end if
  else if $mode_{md_{k-1}} = 1$ **then**
    if $E_1 = 0$ and $E_4 = 1$ or $E_5 = 1$ **then**
      $mode_{md_k} \leftarrow 0$
    else if $E_1 = 1$ and $E_4 = 1$ **then**
      $mode_{md_k} \leftarrow 2$
    else if $E_1 = 1$and $E_4 = 0$ **then**
      $mode_{md_k} \leftarrow 3$
    else
      $mode_{md_k} \leftarrow mode_{md_{k-1}}$
    end if
  else if $mode_{md_{k-1}} = 2$ **then**
    if $E_2 = 1$ and $E_3 = 0$ **then**
      $mode_{md_k} \leftarrow 0$
    else if $E_2 = 1$ and $E_3 = 1$ and $E_6 = 1$ **then**
      $mode_{md_k} \leftarrow 1$
    else if $E_2 = 0$ and $E_3 = 1$ and $E_6 = 1$ **then**
      $mode_{md_k} \leftarrow 3$
    else
      $mode_{md_k} \leftarrow mode_{md_{k-1}}$
    end if
  else if $mode_{md_{k-1}} = 3$ **then**
    if $E_2 = 1$ and $E_4 = 1$ or $E_5 = 1$ **then**
      $mode_{md_k} \leftarrow 0$
    else if $E_2 = 1$ and $E_4 = 0$ **then**
      $mode_{md_k} \leftarrow 1$
    else if $E_2 = 0$ and $E_4 = 1$ **then**
      $mode_{md_k} \leftarrow 2$
    else
      $mode_{md_k} \leftarrow mode_{md_{k-1}}$
    end if
  end if
else if $SOC_{BAT_k} \leq 15$ **then**
  $mode_{md_k} \leftarrow 0$
  $mode_{ro_k} \leftarrow 0$
end if

Algorithm 2 Control of heat exchanger valve position.

if $mode_{md_{k-1}} = 0$ or $mode_{md_{k-1}} = 2$ **then**
  $vp_k \leftarrow 1$
else
  if $|T_{md,in_{k-1}} - 80\,°C| \leq 0.2$ **then**
    $vp_k \leftarrow vp_{k-1}$
  else
    $vp_k \leftarrow vp_{k-1} + 0.01 \cdot \text{sign}(T_{md,in_{k-1}} - 80\,°C$
    $vp_k \leftarrow \max(0, \min(vp_k, 1))$
  end if
end if

Algorithm 3 Logic of operation of RO and MD systems.

if $mode_{RO_k} = 0$ **then**
  $\dot{V}_{RO_k} \leftarrow 0$
  $\dot{m}_{f_k} \leftarrow 0$
else
  if $T_{out_{k-1}} \leq 30\,°C$ **then**
    $\dot{V}_{RO_k} \leftarrow 10\,m^3/h$
    $\dot{m}_{f_k} \leftarrow \frac{\dot{V}_{RO_k}}{n_{PVT}} \cdot \frac{\rho_{sw_k}}{3600}$
  else
    $\dot{m}_{f_k} \leftarrow \left(\dot{V}_{RO_k} - \frac{(T_{out_{k-1}} - 30) \cdot \dot{V}_{RO_k}}{T_{out_{k-1}} - T_{sw_{k-1}}} \right) \cdot \frac{\rho_{sw_k}}{3600 \cdot n_{PVT}}$
    if $\dot{m}_{f_k} < 0.03\,kg$ **then**
      $\dot{m}_{f_k} \leftarrow 0.03\,kg/s$
    end if
    $\dot{V}_{RO_k} \leftarrow 10\,m^3/h$
  end if
end if

Table 11
Cost of main components of the systems.

Component	System A [USD]	System B [USD]	Note
ST collector	410,553.0		3732.3 USD/unit
PV panel	5826.2	–	171.4 USD/unit
PV/T panel	–	31,924.2	760.1 USD/unit
Inverter	4726.1		2363.1 USD/unit
Batteries	23,417.9		5854.5 USD/unit
Heat exchangers	6600.0		2000 USD/m^2 [48]
Thermal storage	51,315.9		17,105.3 USD/unit [49]
Brine tank	8019.9		–
RO unit	85,000.0		[50]
MD module	49,000.0		7000.0 USD/unit [48]
MD membrane	16,354.8		90 USD/m^2 [51]
Pumping system	3335.9		–

In desalination plants corresponding to System A and System B, there are two main sections: the electrical section, which powers the RO and MD units, and the thermal section, which powers the MD units. The calculation of CO_2 emissions avoided consists of determining the annual electrical energy required by the desalination units and the thermal energy required by the heat exchanger of the MD units, under the assumption that the desalination system is powered by conventional energy sources (i.e., the electrical grid for electricity and a condensing boiler for thermal energy). The amount of water production is taken from simulation results. We calculated the thermal energy demand at the heat exchanger, since in the presence of a boiler there is no need for a thermal storage tank or solar thermal collector.

The mass of CO_2 saved, in kg, is calculated for each system as:

$$M_{CO_{2_{el}}} = cde_{el} \cdot E_{el}, \tag{38}$$

Table 12
Summary of system costs.

Parameter	System A	System B	Note
Components cost C_c	664,149.5 USD	690,247.6 USD	$\sum_{i=1}^{N} C_{ci}$ [a]
Installation cost C_{in}	166,037.4 USD	172,561.9 USD	$0.3 \cdot C_c$
Instrumentation cost C_{st}	166,037.4 USD	172,561.9 USD	$0.3 \cdot C_c$
Direct capital cost C_{dc}	996,224.3 USD	1,035,371.3 USD	$C_c + C_{in} + C_{st}$
Indirect capital cost C_{ic}	99,622.4 USD	103,537.1 USD	$0.1 \cdot C_{dc}$
Total capital cost C_{cap}	1,095,846.7 USD	1,138,908.5 USD	$C_{dc} + C_{ic}$
Annual interest rate k	0.03		[50]
Plant lifetime N	25		
Amortization factor a	0.057		[50]
Capital cost annualized C_1	62,932.1 USD	65,405.1 USD	$a \cdot C_{cap}$
Operation and maintenance cost C_2	12,586.4 USD	13,081.0 USD	$0.2 \cdot C_1$
MD membrane replacement cost C_3	2453.2 USD		$0.15 \cdot 90 \cdot A_{md}$ [b] [51]
RO membrane replacement cost C_4	4950.0		[50]
Total annual cost C_{net}	82,921.8 USD	85,889.3 USD	$C_{tot} - R_e$

[a] Cost of each system component [USD].
[b] MD membrane area [m^2].

$$M_{CO_{2_{th}}} = cde_{th} \cdot E_{th}, \tag{39}$$

$$M_{CO_2} = M_{CO_{2_{el}}} + M_{CO_{2_{th}}} \tag{40}$$

where $M_{CO_{2_{el}}}$ is the annual mass of carbon dioxide avoided through the use of photovoltaic energy; cde_{el} is the CO_2 savings coefficient for electricity consumption, determined by the energy mix of the country under analysis (equal to 0.158 kg/kWh for Spain [52]); and E_{el} is the yearly electricity consumption of the plant. Similarly, $M_{CO_{2_{th}}}$ is the annual mass of carbon dioxide avoided through the use of solar thermal energy; cde_{th} is the CO_2 savings coefficient for thermal energy production, with a value of 0.1785 kg/kWh. This coefficient is derived from the higher heating value of methane, accounting for the moles of carbon dioxide produced per mole of methane burned in a condensing boiler, assuming 100% efficiency [52]; and E_{th} is the yearly thermal energy consumption of the plant. Finally, M_{CO_2} represents the total annual CO_2 savings achieved by the desalination system.

3.5. Simulation

System simulations were performed using Python, where the differential equations governing the PV/T units were solved with the odeint solver from the SciPy library. Each simulation step corresponds to a one-minute interval.

The input data of the simulation are the weather conditions of Almería in 2023. Hourly solar radiation and temperature data from PVGis were interpolated to obtain one-minute resolution data. The variation of seawater temperature was considered with one-month resolution, as described in Table 10. The initial weather conditions correspond to those at 00:09 on 1 January 2023, and the following starting conditions were assumed for the systems:

- Temperature on the thermal side of the systems, i.e., the temperature of water in the storage tanks and the hot side of the heat exchanger, equal to 70 °C.
- Temperature of the PV/T layers and the water inside the MD units equal to the ambient seawater temperature.
- Electrical batteries half charged (State of Charge equal to 50%).
- Brine salinity in the tank equal to ambient seawater salinity, with a brine volume of 10 m^3.

Depending on the operation mode, the water flow rate inside the ST units is either equal to the nominal value (0.25 kg/s per loop) or zero. Similarly, the seawater flow rate inside the PV/T is either zero or modulated by the control of the three-way valve, as is the flow rate of water

at the inlet of the heat exchanger. The brine flow rate from the tank to the MD units, depending on the operation mode, is either equal to the nominal value (1.1 m^3/h, as stated in Table 2) or zero.

3.6. Limits of the study

The present work is subject to the following limitations:

- The equations used to calculate the RR and the Specific Energy Consumption (SEC) of the RO process are taken from case studies presented in two different references. The RR data are sourced from Agashichev et al. [36], who considered a seawater salinity of 45,000 ppm, while the SEC data are derived from Koutsou et al. [37], based on a salinity of 40,000 ppm. However, the simulations conducted in this study assume an average Mediterranean seawater salinity of 37,000 ppm [53].
- An increase in seawater temperature during RO operation leads to a higher concentration of salts in the permeate [37]. Consequently, the water quality produced by System B is expected to be lower than that of System A. This aspect has not been addressed in the present analysis.
- The preheating of seawater inside the PV/T unit may introduce issues that are not fully considered in our analysis. For example, scaling and fouling phenomena may occur as seawater temperature increases, potentially damaging both the RO membrane and the channels of the PV/T collector. However, the system has been designed to ensure that the RO feed seawater does not exceed 30 °C, thereby minimizing these risks.
- The corrosive effects of heated seawater inside the PV/T channels have not been considered in this analysis. More generally, the analysis does not account for shutdown periods due to system maintenance, which may lead to an overestimation of freshwater production and an underestimation of water cost.
- The analysis presented in this article has not been validated experimentally, as we are proposing an innovative concept that has not yet been implemented. Nonetheless, the component models adopted from the literature have been validated by their respective authors. For each component described in the article, we provide the reference to the paper in which the model was originally proposed or validated.

4. Results and discussion

The objective of the simulation is to evaluate the monthly freshwater output from RO, MD, and combined RO + MD processes, determine the annual RR of the desalination systems, and quantify the electrical energy generated by the solar panels. Once these quantities have been determined, System A and System B can be compared and the LCOW can be calculated.

4.1. Reverse osmosis production

The monthly RO freshwater production for System A and System B is presented in Fig. 5. The same figure also illustrates the increase in freshwater production by System B compared to System A.

The amount of water produced by System B is consistently greater than that produced by System A. This difference is attributed to three key factors:

- Higher electricity generation: The PV/T system in System B generates more electrical energy than the PV system in System A. This is due to the greater efficiency of PV/T panels, which benefit from the cooling effect of seawater flowing through them. As a result, the RO unit in System B can operate for longer periods than in System A.
- Improved RR: The RO unit in System B achieves a higher RR compared to System A. This is because the seawater passing through the PV/T panels is preheated, enhancing the RO process efficiency.

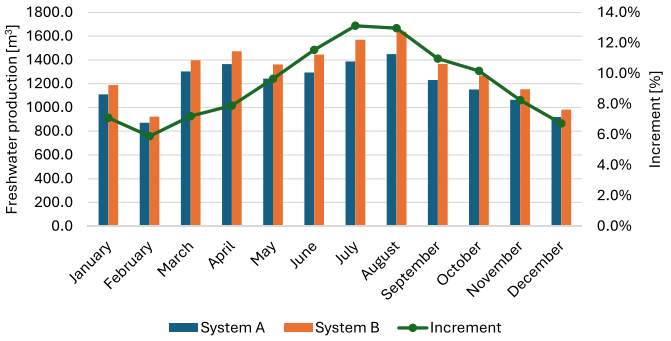

Fig. 5. Monthly RO freshwater output from Systems A and B, and the production increase of System B relative to System A.

The RR associated with year round freshwater production is equal to 40.50% for System A and 42.04% for System B.

- Lower specific energy consumption: Higher seawater temperatures lead to reduced specific electrical consumption in the RO process. This enables the desalination unit in System B to operate for extended durations, further increasing water output.

The yearly freshwater production by RO is equal to 14,395.74 m^3 for System A and to 15,770.10 m^3 for System B with an increment of production equal to 9.55%. The increase in production reaches its peak during the summer and its lowest point in winter. This seasonal variation is primarily due to the enhanced cooling effect on the photovoltaic cells in the PV/T system during summer months, which boosts the efficiency of the panels and extends the RO unit's operating time. The smallest increase in production occurs in February (5.89%), while the highest is recorded in July (13.13%).

It is worth noting that, for the reasons discussed in Section 3.6, the RO production is underestimated. This is because the actual water salinity is lower than the salinity level used during the characterization of the RO RR.

The monthly variation of RO RR is presented in Fig. 6.

As previously described, the RO RR increases with rising seawater temperature. Consequently, the RO RR is higher in summer than in other seasons. The difference in RR between System B and System A becomes more pronounced during months with stronger solar radiation, as the seawater reaches higher temperatures (though always limited to a maximum of 30 °C). The RR associated with RO reaches its maximum in August (45.36% for System A and 47.37% for System B) and minimum in February (37.09% for System A and 37.91% for System B) as shown in Fig. 6.

These results refer specifically to the climate conditions of Almería, Spain. In different climates, the outcomes would change. In warmer

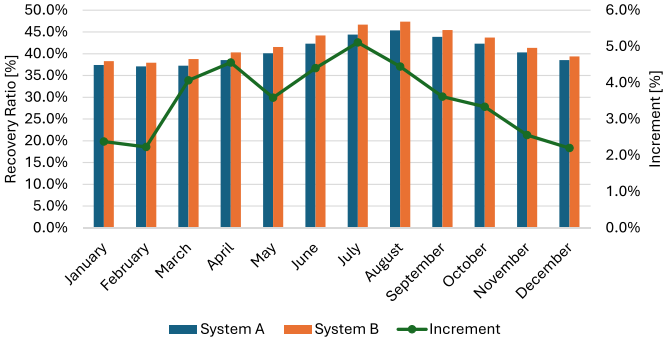

Fig. 6. Monthly RO RR from Systems A and B, and the RR increase of System B relative to System A.

regions, such as tropical areas, the seawater temperature is generally higher and more stable throughout the year compared to the Mediterranean. This would increase the RO RR, leading to greater freshwater production for System A. For System B, however, higher seawater temperatures would reduce the cooling effect on the PV/T panels during summer, lowering their electrical efficiency compared to Mediterranean conditions and thus decreasing the amount of electricity generated. At the same time, tropical coastal regions typically receive higher and more stable solar radiation, which would counterbalance this effect by increasing PV/T energy production. A mirrored situation occurs at higher latitudes. For System A, the RO RR would decrease due to lower seawater temperatures, and RO production would also be limited by reduced solar radiation. For System B, cooler seawater would improve the electrical efficiency of the PV/T panels, but this gain would hardly compensate for the significantly lower solar radiation, ultimately resulting in reduced freshwater production.

4.2. Membrane distillation production

The monthly MD freshwater production for both System A and System B is shown in Fig. 7. The figure also highlights the increase in MD freshwater output achieved by System B relative to System A.

The yearly freshwater production by MD is slightly higher in System B compared to System A. Over the course of the year, System A produces 1327.62 m^3, while System B reaches 1356.84 m^3. This corresponds to a production increase of 2.20% in favor of System B.

The RR of the MD process is nearly identical between System A and System B, measuring 6.28% and 6.24% respectively. This indicates that both systems operate under similar conditions. RR associated with System B is slightly lower because of the higher salinity of feed water due to higher RR of RO operating under higher temperature.

The difference in freshwater production is primarily due to the larger volume of brine generated by System B, which results from its longer operational time of the RO unit.

Fig. 7 shows that MD production reaches its peak in March and April. This can be attributed to several factors. Firstly, these months experience high solar radiation, as reported in Fig. 4, which enables both MD and RO systems to operate for extended periods. Secondly the seawater temperature remains relatively low, resulting in a reduced RO RR. This leads to increased brine production, and the lower brine temperatures at the MD inlet enhance permeate generation, as described by Eq. (21) [39]. Thirdly, brine accumulated during February, when solar radiation was insufficient for longer MD operation, is subsequently treated in March, when solar conditions improve.

Fig. 7 also shows that the smallest production increment occurs in March and April. In April the increment is even negative (−0.41%), meaning that the MD production by System A is higher than production by System B. This is because the increase in RO RR in System B results in a lower brine flow rate compared to System A that is not compensated by longer RO operation time.

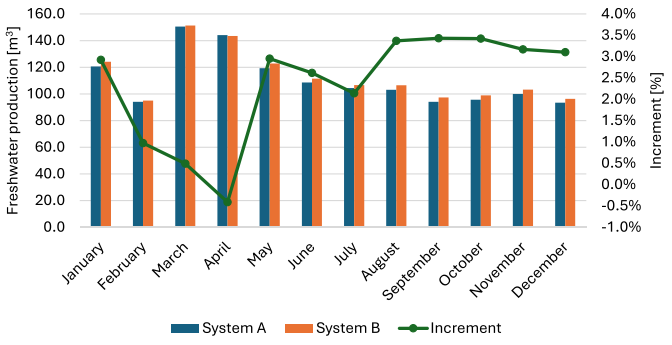

Fig. 7. Monthly MD freshwater output from Systems A and B, and the production increase of System B relative to System A.

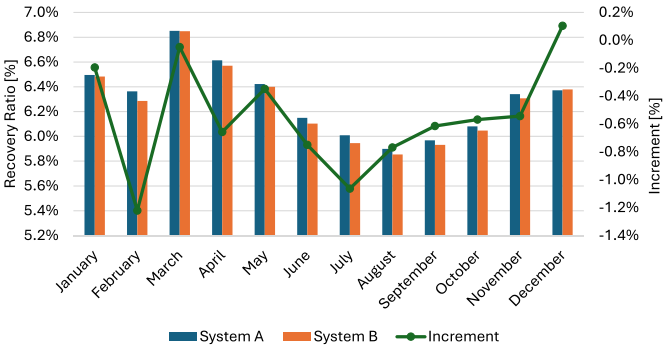

Fig. 8. Monthly MD RR from Systems A and B, and the RR increase of System B relative to System A.

Fig. 8 shows the monthly variation of MD RR.

The MD RR is related to the RO RR: it decreases during the summer (5.90% for System A and 5.85% for System B in August) due to higher brine salinity resulting from the increased RO RR caused by elevated seawater temperature. Moreover, the higher RO brine temperature in summer leads to a lower permeate flux in MD. These factors also explain why the RR of System A is higher than that of System B: the latter operates with higher seawater temperatures, which produce brine of greater salinity and temperature. Feed salinity and temperature have a significant influence on MD performance, as demonstrated by [39]. The MD RR increases in March (6.85% for both System A and B) because of the higher water temperature at the outlet of the heat exchanger, i.e., at the MD inlet ($T_{md,in}$), due to strong solar radiation, while the RO brine temperature remains relatively low.

MD production and RR are strongly influenced by climatic conditions. In coastal tropical regions, higher RO brine temperatures and higher brine salinity are expected, which tend to reduce the MD RR. This effect is particularly relevant for System A, where the RO seawater inlet temperature is not regulated by a three-way valve. Tropical coastal areas also experience more stable and generally higher solar radiation compared to Mediterranean regions. This leads to greater freshwater production in both System A and System B; however, the increase in production does not correspond to an increase in MD RR. At higher latitudes, the opposite situation occurs: seawater is cooler and typically less saline. Lower salinity should enhance MD RR, and the reduced temperature at the cold MD inlet also contributes positively. Nevertheless, the lower solar radiation decreases the temperature at the hot MD inlet, counteracting these benefits. In other words, to accurately quantify the impact of reduced solar radiation on RR, further simulations would be necessary. What is clear, however, is that lower annual solar radiation inevitably results in reduced freshwater production.

4.3. Overall desalination production

The results of overall desalination production, i.e., the production from the combination of RO and MD, are reported in Fig. 9.

The annual freshwater production achieved by System A is 15,723.36 m^3, whereas System B produces 17,126.94 m^3 i.e., an increase of 8.93% in yearly output. These results indicate that the use of a PV/T collector leads to higher freshwater production compared to a system equipped with only PV under identical conditions. However, Table 12 shows that the capital cost of System B is higher than that of System A. A detailed economic comparison between the two systems will be presented in Section 4.5.

The implementation of MD for brine valorization results in an increase in freshwater production compared to that achieved by the RO unit alone. For System A, this annual increase amounts to 9.22%, while

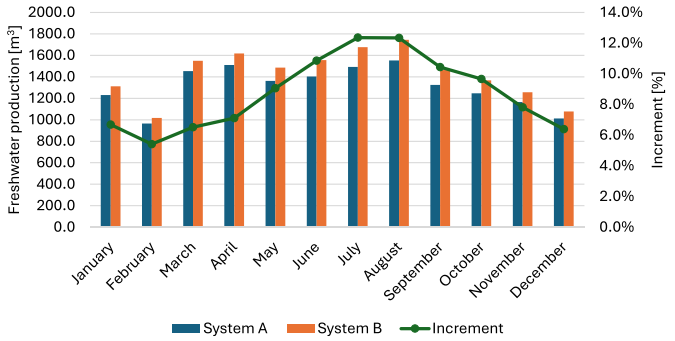

Fig. 9. Monthly RO-MD freshwater output from Systems A and B, and the production increase of System B relative to System A.

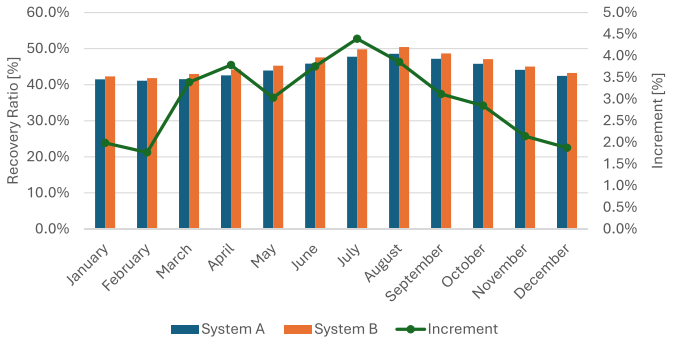

Fig. 10. Monthly global RR from Systems A and B, and the RR increase of System B relative to System A.

for System B it is 8.60%. This desalination strategy also enhances the RR: the overall RR associated with the desalination process in System A is 44.23%, and in System B it reaches 45.66%. These values are higher than those obtained from RO operation alone, which are 40.50% and 42.04% for System A and System B, respectively. These findings also indicate that System B enables more efficient freshwater production compared to System A. The higher efficiency associated to System B is predominantly related to the increase of RO RR associated to the heating of seawater in PV/T collectors.

The monthly increase in freshwater production follows a trend similar to that observed for RO freshwater output, due to the dominant contribution of RO compared to MD. The smallest increase in freshwater production by System B relative to System A occurs in February (5.41%), while the largest is recorded in July (12.36%).

The annual volume of seawater treated is 35,549.33 m^3 for System A and 37,509.00 m^3 for System B. Based on the previously mentioned RRs (RR), the results indicate that adopting a tandem configuration (RO-MD) enables the avoidance of brine discharge amounting to 1327.62 m^3 and 1356.84 m^3 for System A and System B, respectively. These findings demonstrate that the RO-MD configuration not only facilitates RO brine valorization but also contributes to a reduction in the final volume of discharged brine.

It is reiterated that the RO water production is underestimated. Consequently, the MD water production and the overall water output are also underestimated, for reasons previously discussed.

Fig. 10 shows the monthly variation of whole systems RR.

RR of the whole system depends more strongly on RO RR than on MD RR, since the volume of water produced by the RO unit is much higher. Therefore, the global RR follows a trend similar to that of the RO RR. The increment of RR related to System B with respect to System A is always positive, reaching a maximum of 4.40% in July. As expected, the maximum increment occurs during the summer, when seawater

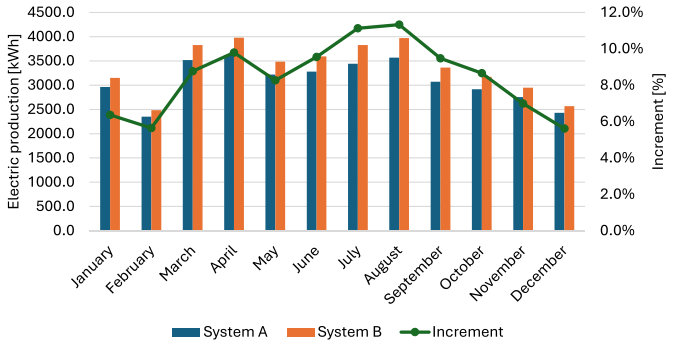

Fig. 11. Monthly electric energy production from Systems A and B, and the production increase of System B relative to System A.

preheating inside the PV/T panels allows the RO unit to operate with higher RR.

The influence of different climate conditions on overall freshwater production aligns with the observations discussed earlier. Since total production depends primarily on solar energy availability, coastal tropical regions are expected to achieve higher freshwater output, as well as higher electrical and thermal energy generation, which in turn drives freshwater production. However, the behavior of the RR across different climates is less straightforward. Because the overall system RR is strongly influenced by the RO stage, one might expect that the higher RO RR typically observed in warmer regions would lead to higher overall RR for both Systems A and B. Yet, these considerations are not currently supported by simulation or experimental data, indicating the need for more detailed studies on this topic.

4.4. Electric production

The monthly results of electrical energy production by System A and System B is reported in Fig. 11.

Although System A and System B are designed to deliver the same power under Standard Test Conditions (STC), their actual annual electric output differs. The yearly energy produced by the PV panels is 37.144 MWh, whereas the PV/T panels generate 40.369 MWh, i.e., an increase of 8.7%. This difference is attributed to the higher operating efficiency of photovoltaic cells in the PV/T system compared to the PV system, due to the cooling effect of seawater flowing through the hybrid panel.

The monthly increase in electricity production is more pronounced during the summer months, when the cooling effect of seawater has a greater impact owing to elevated cell temperatures caused by higher ambient temperatures and solar radiation. The smallest increase occurs in February (5.64%), while the largest is observed in August (11.33%).

4.5. Economic and environmental analysis results

A brief summary of results obtained by analysis is reported in Table 13. In the same table the values of LCOW for System A and System B are reported.

Although the capital cost associated with System B is higher than that of System A, the resulting LCOW is lower, amounting to 5.27 USD/m^3 for System A and 5.01 USD/m^3 for System B. This reduction is primarily due to the significantly greater freshwater production achieved by System B compared to System A.

Water production is underestimated, which in turn leads to an overestimation of the LCOW from this perspective. However, this study does not account for shutdown periods due to maintenance or breakdowns, an omission that, conversely, results in an underestimation of LCOW.

The calculated LCOW values are lower than those reported for several comparable standalone renewable-powered systems. For example,

Table 13
Overall annual performance of Systems A and B, and the improvement of System B relative to System A.

Quantity	System A	System B	Increment
Water produced by RO	14,395.74 m^3	15,770.10 m^3	9.55%
Water produced by MD	1327.62 m^3	1356.84 m^3	2.20%
Water produced by RO + MD	15,723.36 m^3	17,126.94 m^3	8.93%
RO RR	40.50%	42.04%	3.82%
MD RR	6.28%	6.24%	−0.55%
RO + MD RR	44.23%	45.66%	3.24%
Electric energy generation	37.144 MWh	40.369 MWh	8.68%
LCOW	5.27 USD/m^3	5.01 USD/m^3	−4.91%
$M_{CO_{2_{el}}}$ [ton] saved	5.87	6.33	7.80%
$M_{CO_{2_{th}}}$ [ton] saved	23.31	22.57	−3.17%
M_{CO_2} [ton] saved	29.18	28.90	−0.97%

Al Obaidi et al. and Sadhwani et al. report water costs for small-scale PV-RO systems ranging from 11.7 to 15.6 USD/m^3 [54,55]. Ayou et al. [34] conducted a feasibility study on a small-scale PV-RO system, achieving a LCOW of 9.0 USD/m^3. ST-driven MD systems are reported to cost between 15 and 18 USD/m^3 [11]. Even higher water costs for ST-MD desalination systems are reported by Jawed et al. [56]. Renewable-based desalination systems exhibit a wide range of water costs, primarily due to system complexity and the varying methodologies used to evaluate individual cost components.

In the case of PV-RO systems, some studies report LCOW values lower than those found in this work [57]. While storage systems can extend operational time and increase water output, their high costs (5322.20 USD/unit for electric storage and 17,105.30 USD/unit for thermal storage) have a dual effect: they enhance performance but significantly raise capital investment, thereby increasing the overall water cost. Moreover, the high cost of ST and PV/T modules, along with MD units, results in elevated capital expenditures, leading to a higher LCOW compared to RO systems powered solely by PV. Additionally, the LCOW of the proposed systems remains higher than that of conventional desalination technologies. For instance, Gökçek et al. [58] reported costs ranging from 1.489 to 1.750 USD/m^3 for small-scale RO systems powered exclusively by the electric grid, while Curto et al. [7] reported values between 0.45 and 1.72 USD/m^3.

Although the LCOW of the systems presented in this study is higher than that reported in some previous works on solar-powered desalination [15,57], the primary aim of our research was not to propose a more cost-effective solution than those found in the literature. Instead, our main objective was to demonstrate the technical and economic feasibility, as well as the advantages, of double-stage desalination systems for brine valorization compared to the use of RO alone. A secondary objective was to investigate the integration of PV/T panels in place of conventional PV panels, emphasizing their benefits in terms of economics, water production, and RR. These aspects have been thoroughly discussed in the previous sections, showing that the adoption of a double-stage desalination system leads to increased water production, RR and decreased brine discharge, while the use of PV/T panels instead of PV results in improved overall performance and greater cost-effectiveness. Finally, it is important to note that storage systems enable the proposed desalination systems to produce freshwater even without sunlight. This capability, along with reduced brine discharge, provides added value compared to simpler PV-RO systems in the literature, which, despite lower LCOW, lack such advantages.

Results of the environmental analysis are presented in Table 13. The comparison of CO_2 savings between System A and System B, relative to a desalination system powered by conventional energy sources with the same output, shows that System B achieves lower overall savings. This outcome is primarily due to the large share of thermal energy required by both systems, which accounts for most of the carbon dioxide savings. Specifically, the thermal energy demand of System A is higher than that of System B, even though the MD water production in System A is lower. This difference arises from the model proposed by Andrés-Mañas et al. [39], which we adopted, where the specific thermal energy consumption (STEC) decreases slightly as the inlet temperature $T_{sw,h}$ of the MD units increases. In System B, this inlet temperature is raised through RO seawater preheating provided by PV/T panels. Conversely, the CO_2 savings associated with electrical energy consumption are greater in System B than in System A. This is explained by the larger amount of electricity generated by PV/T panels, enhanced by the cooling effect of seawater.

The amount of carbon dioxide saved is significant and highlights the benefits of scaling the proposed systems. However, these savings would be reduced if the environmental analysis compared System A and System B with a desalination system composed solely of RO units with same amount of water production.

It is important to note that the environmental analysis was carried out in a European country (Spain) where carbon dioxide emissions are relatively low due to an energy mix in which renewable sources play a significant role. Performing the same analysis in other regions, such as the Middle East or the United States, would likely result in greater environmental benefits, since the baseline carbon dioxide emissions associated with the local energy mix would be higher, and thus the reduction achieved by the system would be more substantial.

5. Conclusion

To address the environmental impact of desalination and improve resource recovery through brine valorization, this study proposes, analyzes, and compares two solar-powered desalination systems with energy storage. Both configurations combine MD units operating in series with an RO unit. The first system uses PV panels and ST collectors, while the second integrates PV/T panels with ST collectors. Simulations are conducted over a full year using real meteorological data from Almería, Spain. A key objective is to demonstrate the superior performance and viability of PV/T technology in desalination applications highlighting its potential to improve RR, water production, and energy efficiency. The study also evaluates the systems' ability to operate entirely on solar energy and compares water production costs to literature benchmarks to assess economic feasibility.

The RO-MD tandem configuration has been shown to enhance both RR and freshwater output. In System A, production increases by 9.22% compared to RO alone, yielding 15,723.36 m^3 of freshwater. System B shows an 8.60% increase, reaching 17,126.94 m^3. The RR in System A rises from 40.50% (RO) to 44.23% (RO-MD), and in System B from 42.04% to 45.66%.

The results showed that using PV/T in System B improves overall production. Preheating the seawater boosts RO RR (RR), reduces specific energy consumption (SEC), and increases PV cell efficiency, resulting in lower energy use, greater energy output, and longer operating time compared to System A. This leads to a production increment equal to 8.93% with an increase of RR equal to 3.24%.

Although the annualized cost of System B is higher than that of System A, its LCOW is lower, 5.01 and 5.27 USD/m^3, respectively. This is attributed to the greater freshwater production achieved by System B. While these values remain above the cost of freshwater produced using conventional energy sources, they are lower than many values reported in the literature for solar-powered desalination systems.

Although the LCOW of our systems is higher than in some previous studies, our goal was not cost minimization but to demonstrate the technical and economic feasibility of double-stage desalination for brine valorization versus RO alone. We also examined PV/T panels over PV, showing benefits in economics, water production, and RR. As discussed, double-stage systems increase water output, recovery, and reduce brine discharge, while PV/T improves overall performance and

cost-effectiveness. Finally, storage enables freshwater production without sunlight, adding value beyond simpler PV-RO systems that, despite lower LCOW, lack these advantages.

Finally, the environmental analysis shows that System B achieves lower overall CO_2 savings due to the high thermal energy demand in both systems while System A requires more thermal energy despite its lower MD output. Conversely, System B attains greater CO_2 savings from electricity, thanks to higher PV/T generation enhanced by seawater cooling.

5.1. Future works

The proposed study suggests several possible directions for future work, including

- developing an experimental setup to validate the results obtained through simulation;
- performing a complete experimental characterization of the RO unit to obtain more accurate results when integrating it into the system model;
- considering plant shutdown periods in the evaluation of LCOW and freshwater production;
- assessing the quality of the water produced by the desalination systems;
- investigating the concept of deploying multiple MD units in series to further enhance the system's RR;
- optimizing the design and operation of proposed systems to maximize RR and freshwater output and to minimize water cost.

CRediT authorship contribution statement

Paolo Vitulli: Writing – original draft, Software, Methodology, Investigation, Data curation, Conceptualization. **Alejandro Bueso Sánchez:** Writing – review & editing, Software, Methodology, Investigation, Data curation, Conceptualization. **Giulia Tanoni:** Writing – review & editing, Supervision. **Emanuele Principi:** Writing – review & editing, Visualization, Supervision. **Stefano Squartini:** Writing – review & editing, Visualization, Supervision. **Guillermo Zaragoza:** Writing – review & editing, Visualization, Supervision, Conceptualization.

Declaration of generative AI and AI-assisted technologies in the writing process

During the preparation of this work the authors used Microsoft Copilot and ChatGPT in order to improve the readability and language of the manuscript. After using this tool/service, the authors reviewed and edited the content as needed and take full responsibility for the content of the published article.

Declaration of competing interest

The authors declare that they have no known competing financial interests or personal relationships that could have appeared to influence the work reported in this paper.

Data availability

The data that has been used is confidential.

References

[1] UNESCO World Water Assessment Programme, The United Nations World Water Development Report 2024: Water for Prosperity and Peace, UNESCO, 2024.

[2] EU Blue Economy Observatory, Desalination, 2025, https://blue-economy-observatory.ec.europa.eu/eu-blue-economy-sectors/desalination_en (accessed on 24 February 2025).

[3] European Environment Agency, Water scarcity conditions in Europe, 2025, https://www.eea.europa.eu/en/analysis/indicators/use-of-freshwater-resources-in-europe-1 (accessed on 24 February 2025).

[4] E. Jones, M. Qadir, M.T.H. van Vliet, V. Smakhtin, S. mu Kang, The state of desalination and brine production: a global outlook, Sci. Total Environ. 657 (2019) 1343–1356, https://doi.org/10.1016/j.scitotenv.2018.12.076, https://www.sciencedirect.com/science/article/pii/S0048969718349167.

[5] M.À. Martínez Medina, M.Á. Pérez Martín, T. Estrela, Desalination in Spain and the role of solar photovoltaic energy, J. Mar. Sci. Eng. 12 (6) (2024), https://doi.org/10.3390/jmse12060859, https://www.mdpi.com/2077-1312/12/6/859.

[6] F. Calise, F.L. Cappiello, R. Vanoli, M. Vicidomini, Economic assessment of renewable energy systems integrating photovoltaic panels, seawater desalination and water storage, Appl. Energy 253 (2019) 113575, https://doi.org/10.1016/j.apenergy.2019.113575, https://www.sciencedirect.com/science/article/pii/S0306261919312498.

[7] D. Curto, V. Franzitta, A. Guercio, A review of the water desalination technologies, Applied Sci. 11 (2) (2021), https://doi.org/10.3390/app11020670, https://www.mdpi.com/2076-3417/11/2/670.

[8] W. He, G. Huang, C.N. Markides, Synergies and potential of hybrid solar photovoltaic-thermal desalination technologies, Desalination 552 (2023) 116424, https://doi.org/10.1016/j.desal.2023.116424, https://www.sciencedirect.com/science/article/pii/S0011916423000565.

[9] S. Shalaby, S.W. Sharshir, A.E. Kabeel, A.W. Kandeal, H.F. Abosheiasha, M. Abdelgaied, M.H. Hamed, N. Yang, Reverse osmosis desalination systems powered by solar energy: preheating techniques and brine disposal challenges – a detailed review, Energy Convers. Manag. 251 (2022) 114971, https://doi.org/10.1016/j.enconman.2021.114971, https://www.sciencedirect.com/science/article/pii/S019689042101147X.

[10] A. Prado de Nicolás, Á. Molina-García, J.T. García-Bermejo, F. Vera-García, Desalination, minimal and zero liquid discharge powered by renewable energy sources: current status and future perspectives, Renew. Sustain. Energy Rev. 187 (2023) 113733, https://doi.org/10.1016/j.rser.2023.113733, https://www.sciencedirect.com/science/article/pii/S1364032123005907.

[11] B. Tashtoush, W. Alyahya, M. Al Ghadi, J. Al-Omari, T. Morosuk, Renewable energy integration in water desalination: state-of-the-art review and comparative analysis, Appl. Energy. 352 (2023) 121950, https://doi.org/10.1016/j.apenergy.2023.121950, https://www.sciencedirect.com/science/article/pii/S0306261923013144.

[12] A.I. Dawahdeh, M.A. Al-Nimr, T.N. Al-Sarhan, Performance evaluation for a high temperature alkaline fuel cell integrated with thermal vapor compression desalination, Appl. Energy. 377 (2025) 124691, https://doi.org/10.1016/j.apenergy.2024.124691, https://www.sciencedirect.com/science/article/pii/S0306261924020749.

[13] Z. Wu, X. Zhao, Y. Mao, R. Liu, Flexibility quantification of desalination plants for demand response: an adaptive robust optimization methodology, Appl. Energy 373 (2024) 123835, https://doi.org/10.1016/j.apenergy.2024.123835, https://www.sciencedirect.com/science/article/pii/S0306261924012182.

[14] V.G. Gude, Energy storage for desalination processes powered by renewable energy and waste heat sources, Appl. Energy 137 (2015) 877–898, https://doi.org/10.1016/j.apenergy.2014.06.061, https://www.sciencedirect.com/science/article/pii/S0306261914006436.

[15] E.M. Almetwally, M.A. Elazab, A.E. Kabeel, Y. Yasser, A. Elgebaly, Solar powered Reverse Osmosis desalination: a systematic review of technologies, integration strategies and challenges, Desalination 615 (2025) 119228, https://doi.org/10.1016/j.desal.2025.119228, https://www.sciencedirect.com/science/article/pii/S0011916425007040.

[16] M. Kettani, P. Bandelier, Techno-economic assessment of solar energy coupling with large-scale desalination plant: the case of Morocco, Desalination 494 (2020) 114627, https://doi.org/10.1016/j.desal.2020.114627, https://www.sciencedirect.com/science/article/pii/S0011916420313059.

[17] J.A. Andrés-Mañas, L. Roca, A. Ruiz-Aguirre, F.G. Acién, J.D. Gil, G. Zaragoza, Application of solar energy to seawater desalination in a pilot system based on vacuum multi-effect membrane distillation, Appl. Energy 258 (2020) 114068, https://doi.org/10.1016/j.apenergy.2019.114068, https://www.sciencedirect.com/science/article/pii/S0306261919317556.

[18] E.M. Almetwally, M. El Hadi Attia, M. Elazab, M. Bassyouni, A.E. Kabeel, Improving thermal efficiency and water production in conical solar stills through integrating pistachio shells and paraffin wax phase change material, Energy Convers. Manag. 346 (2025) 120462, https://doi.org/10.1016/j.enconman.2025.120462, https://www.sciencedirect.com/science/article/pii/S0196890425009860.

[19] A. Panagopoulos, Brine management (saline water & wastewater effluents): sustainable utilization and resource recovery strategy through minimal and zero liquid discharge (MLD & zld) desalination systems, Chem. Eng. Process. - Process Intensif. 176 (2022) 108944, https://doi.org/10.1016/j.cep.2022.108944, https://www.sciencedirect.com/science/article/pii/S025527012200157X.

[20] M. Yaqub, W. Lee, Zero-liquid discharge (zld) technology for resource recovery from wastewater: a review, Sci. Total Environ. 681 (2019) 551–563, https://doi.org/10.1016/j.scitotenv.2019.05.062, https://www.sciencedirect.com/science/article/pii/S0048969719320741.

[21] J.-P. Mericq, S. Laborie, C. Cabassud, Vacuum membrane distillation of seawater reverse osmosis brines, Water Res. 44 (18) (2010) 5260–5273, https://doi.org/10.1016/j.watres.2010.06.052, https://www.sciencedirect.com/science/article/pii/S0043135410004392.

[22] H.S. Son, S. Soukane, J. Lee, Y. Kim, Y.-D. Kim, N. Ghaffour, Towards sustainable circular brine reclamation using seawater reverse osmosis, membrane distillation and forward osmosis hybrids: an experimental investigation, J. Environ. Manag. 293 (2021) 112836, https://doi.org/10.1016/j.jenvman.2021.112836, https://www.sciencedirect.com/science/article/pii/S0301479721008987.

[23] M.T.T. Ngo, B.Q. Diep, H. Sano, Y. Nishimura, S. Boivin, H. Kodamatani, H. Takeuchi, S.C.W. Sakti, T. Fujioka, Membrane distillation for achieving high water recovery for potable water reuse, Chemosphere 288 (2022) 132610, https://doi.org/10.1016/j.chemosphere.2021.132610, https://www.sciencedirect.com/science/article/pii/S0045653521030824.

[24] M. Herrando, K. Wang, G. Huang, T. Otanicar, O.B. Mousa, R.A. Agathokleous, Y. Ding, S. Kalogirou, N. Ekins-Daukes, R.A. Taylor, C.N. Markides, A review of solar hybrid photovoltaic-thermal (pv-t) collectors and systems, Prog. Energy Combust. Sci. 97 (2023) 101072, https://doi.org/10.1016/j.pecs.2023.101072, https://www.sciencedirect.com/science/article/pii/S0360128523000023.

[25] H. Togun, A. Basem, A.A.H. Kadhum, A.M. Abed, N. Biswas, F.L. Rashid, R.A. Lawag, H.M. Ali, H.I. Mohammed, D.K. Mandal, Advancing photovoltaic thermal (pv/t) systems: innovative cooling technique, thermal management, and future prospects, Sol. Energy 291 (2025) 113402, https://doi.org/10.1016/j.solener.2025.113402, https://www.sciencedirect.com/science/article/pii/S0038092X25001653.

[26] B. Anand, R. Shankar, S. Murugavelh, W. Rivera, K. Midhun Prasad, R. Nagarajan, A review on solar photovoltaic thermal integrated desalination technologies, Renew. Sustain. Energy Rev. 141 (2021) 110787, https://doi.org/10.1016/j.rser.2021.110787, https://www.sciencedirect.com/science/article/pii/S1364032121000824.

[27] M. Wiesenfarth, J. Went, A. Bösch, A. Dilger, T. Kec, A. Kroll, J. Koschikowski, A.W. Bett, Cpv-T mirror dish system combined with water desalination systems, AIP Conf. Proc. 1766 (1) (2016) 020008, https://doi.org/10.1063/1.4962076, https://pubs.aip.org/aip/acp/article-pdf/doi/10.1063/1.4962076/13097356/020008_1_online.pdf.

[28] J. Uche, L. Acevedo, F. Círez, S. Usón, A. Martínez-Gracia, Á.A. Bayod-Rújula, Analysis of a domestic trigeneration scheme with hybrid renewable energy sources and desalting techniques, J. Clean. Prod. 212 (2019) 1409–1422, https://doi.org/10.1016/j.jclepro.2018.12.006, https://www.sciencedirect.com/science/article/pii/S0959652618337089.

[29] J. Uche, A. Muzás, L. Acevedo, S. Usón, A. Martínez, A.A. Bayod, Experimental tests to validate the simulation model of a domestic trigeneration scheme with hybrid RESS and desalting techniques, Renewable Energy 155 (2020) 407–419, https://doi.org/10.1016/j.renene.2020.03.147, https://www.sciencedirect.com/science/article/pii/S0960148120304808.

[30] R. Li, S. Zheng, R. Wang, Z. Xu, Energy and exergy analyses of a solar pv/t driving hybrid reverse osmosis-thermal distillation system, Sol. Energy 263 (2023) 111985, https://doi.org/10.1016/j.solener.2023.111985, https://www.sciencedirect.com/science/article/pii/S0038092X23006199.

[31] F. Mahmoudi, D. Ng, K. Ang, Z. Xie, Sustainable desalination through hybrid photovoltaic/thermal membrane distillation: development of an off-grid prototype, Sol. Energy. 284 (2024) 113090, https://doi.org/10.1016/j.solener.2024.113090, https://www.sciencedirect.com/science/article/pii/S0038092X24007850.

[32] M. Ghazy, M.E. Zayed, S. Rehman, K. Irshad, E. Ibrahim, A. Mohamed, E.S. Ali, A.S. Alsaman, R.B. Mansour, R. Ben-Mansour, A.A. Askalany, Dynamic numerical modeling and performance assessment of a hybrid photovoltaic thermal collector adsorption desalination system for sustainable water-energy nexus, Solar Energy 292 (2025) 113441, https://doi.org/10.1016/j.solener.2025.113441, https://www.sciencedirect.com/science/article/pii/S0038092X2500204X.

[33] M. Abdelgaied, M. Fathi Seleem, M. Mahgoub Bassuoni, A.M. Khaira, Performance of a solar hybrid desalination plant integrated with photovoltaic-thermal collectors for remote regions: experimental and modeling investigation, Solar Energy 264 (2023) 112082, https://doi.org/10.1016/j.solener.2023.112082, https://www.sciencedirect.com/science/article/pii/S0038092X23007168.

[34] D.S. Ayou, H.M. Ega, A. Coronas, A feasibility study of a small-scale photovoltaic-powered Reverse osmosis desalination plant for potable water and salt production in Madura Island: a techno-economic evaluation, Therm. Sci. Eng. Prog. 35 (2022) 101450, https://doi.org/10.1016/j.tsep.2022.101450, https://www.sciencedirect.com/science/article/pii/S2451904922002566.

[35] European Commission, Photovoltaic geographical information system (PVGIS), 2025, https://joint-research-centre.ec.europa.eu/photovoltaic-geographical-information-system-pvgis_en (accessed on 6 February 2025).

[36] S.P. Agashichev, K.N. Lootahb, Influence of temperature and permeate recovery on energy consumption of a reverse osmosis system, Desalination 154 (3) (2003) 253–266, https://doi.org/10.1016/S0011-9164(03)80041-3, https://www.sciencedirect.com/science/article/pii/S0011916403800413.

[37] C. Koutsou, E.M. Kritikos, A.J. Karabelas, M. Kostoglou, Analysis of temperature effects on the specific energy consumption in reverse osmosis desalination processes, Desalination 476 (2020) 114213, https://doi.org/10.1016/j.desal.2019.114213, https://www.sciencedirect.com/science/article/pii/S0011916419315607.

[38] T. Mohammadi, M. Kazemi Moghadam, S.S. Madaeni, Hydrodynamic factors affecting flux and fouling during reverse osmosis of seawater, Desalination 151 (3) (2003) 239–245, https://doi.org/10.1016/S0011-9164(02)01016-0, https://www.sciencedirect.com/science/article/pii/S0011916402010160.

[39] J.A. Andrés-Mañas, I. Requena, G. Zaragoza, Membrane distillation of high salinity feeds: steady-state modelling and optimization of a pilot-scale module in vacuum-assisted AIR gap operation, Desalination 553 (2023) 116449, https://doi.org/10.1016/j.desal.2023.116449, https://www.sciencedirect.com/science/article/pii/S0011916423000814.

[40] C. El Fouas, B. Hajji, A. Gagliano, G.M. Tina, S. Aneli, Numerical model and experimental validation of the electrical and thermal performances of photovoltaic/thermal plant, Energy Convers. Manag. 220 (2020) 112939, https://doi.org/10.1016/j.enconman.2020.112939, https://www.sciencedirect.com/science/article/pii/S0196890420304775.

[41] R. Cole, N.S. Sturrock, The convective heat exchange at the external surface of buildings, Build. Environ. 12 (4) (1977) 207–214, https://doi.org/10.1016/0360-1323(77)90021-X, https://www.sciencedirect.com/science/article/pii/036013237790021X.

[42] S.W. Churchill, A comprehensive correlating equation for laminar, assisting, forced and free convection, AIChE J. 23 (1) (1977) 10–16, https://doi.org/10.1002/aic.690230103, https://aiche.onlinelibrary.wiley.com/doi/pdf/10.1002/aic.690230103.

[43] H.B. cheikh el hocine, K. Touafek, F. Kerrour, H. Haloui, A. Khelifa, Model validation of an empirical photovoltaic thermal (pv/t) collector, Energy Procedia 74 (2015) 1090–1099, the International Conference on Technologies and Materials for Renewable Energy, Environment and Sustainability –TMREES15. doi:https://doi.org/10.1016/j.egypro.2015.07.749, https://www.sciencedirect.com/science/article/pii/S1876610215015179.

[44] T.L. Bergman, A.S. Lavine, F.P. Incropera, D.P. DeWitt, Fundamentals of Heat and Mass Transfer, Wiley, 2017.

[45] Dualsun, Technical datasheet - SPRING MAX, 2025, https://dualsun.com/en/professionals/datasheet/spring4-425-topcon-finned (accessed on 16 June 2025).

[46] J.D. Gil, J. Álvarez, L. Roca, J.A. Sánchez-Molina, M. Berenguel, F. Rodríguez, Optimal thermal energy management of a distributed energy system comprising a solar membrane distillation plant and a greenhouse, Energy Convers. Manag. 198 (2019) 111791, https://doi.org/10.1016/j.enconman.2019.111791

[47] Sea Temperature Info, Water temperature in Almeria (Costa De Almeria), 2025, https://seatemperature.info/spain/almeria-water-temperature.html (accessed on 6 February 2025).

[48] G. Mohan, U. Kumar, M.K. Pokhrel, A. Martin, A novel solar thermal polygeneration system for sustainable production of cooling, clean water and domestic hot water in United Arab Emirates: dynamic simulation and economic evaluation, Appl. Energy 167 (2016) 173–188.

[49] J.F. Rosales-Pérez, A. Villarruel-Jaramillo, M. Pérez-García, J.M. Cardemil, R. Escobar, Techno-economic analysis of hybrid solar thermal systems with flat plate and parabolic trough collectors in industrial applications, Alex. Eng. J. 86 (2024) 98–119, https://doi.org/10.1016/j.aej.2023.11.056, https://www.sciencedirect.com/science/article/pii/S1110016823010451.

[50] A.K. Elfaqih, S.O. Belhaj, Economic evaluation of SWRO desalination plants using erd powered by off-grid PV system, in: 2021 IEEE 1st International Maghreb Meeting of the Conference on Sciences and Techniques of Automatic Control and Computer Engineering MI-STA, 2021, pp. 458–462, https://doi.org/10.1109/MI-STA52233.2021.9464492

[51] F. Macedonio, E. Curcio, E. Drioli, Integrated membrane systems for seawater desalination: energetic and exergetic analysis, economic evaluation, experimental study, Desalination 203 (1–3) (2007) 260–276.

[52] P. Vitulli, E. Principi, S. Squartini, G. Tanoni, A. Gagliano, G.M. Tina, Energetic, exergetic, economic and environmental analysis of a photovoltaic/thermal system equipped with thermoelectric generators, Sustain. Energy, Grids Netw. 43 (2025) 101803, https://doi.org/10.1016/j.segan.2025.101803, https://www.sciencedirect.com/science/article/pii/S2352467725001857.

[53] K. Christopoulos, N. Pospotikis, E. Kostopoulos, E. Kondili, J.K. Kaldellis, Experimental analysis of the water salinity impact on the energy consumption of small desalination plants, Procedia Struct. Integr. 10 (2018) 171–178, 1st International Conference of the Greek Society of Experimental Mechanics of Materials, Athens, May 10–12, 2018. doi:https://doi.org/10.1016/j.prostr.2018.09.025, https://www.sciencedirect.com/science/article/pii/S2452321618300738.

[54] M.A. Al-Obaidi, R.H.A. Zubo, F.L. Rashid, H.J. Dakkama, R. Abd-Alhameed, I.M. Mujtaba, Evaluation of solar energy powered seawater desalination processes: a review, Energies 15 (18) (2022), https://doi.org/10.3390/en15186562, https://www.mdpi.com/1996-1073/15/18/6562.

[55] J. Jaime Sadhwani, M. Sagaseta de Ilurdoz, Primary energy consumption in desalination: the case of Gran Canaria, Desalination 452 (2019) 219–229, https://doi.org/10.1016/j.desal.2018.11.004, https://www.sciencedirect.com/science/article/pii/S001191641830122X.

[56] A.S. Jawed, L. Nassar, H.M. Hegab, R. van der Merwe, F. Al Marzooqi, F. Banat, S.W. Hasan, Recent developments in solar-powered membrane distillation for sustainable desalination, Heliyon 10 (11) (2024) e31656, https://doi.org/10.1016/j.heliyon.2024.e31656, https://www.sciencedirect.com/science/article/pii/S2405844024076874.

[57] M.A. Khan, S. Rehman, F.A. Al-Sulaiman, A hybrid renewable energy system as a potential energy source for water desalination using reverse osmosis: a review, Renew. Sustain. Energy Rev. 97 (2018) 456–477, https://doi.org/10.1016/j.rser.2018.08.049, https://www.sciencedirect.com/science/article/pii/S1364032118306336.

[58] M. Gökçek, Ö.B. Gökçek, Technical and economic evaluation of freshwater production from a wind-powered small-scale seawater reverse osmosis system (wp-swro), Desalination 381 (2016) 47–57, https://doi.org/10.1016/j.desal.2015.12.004